SYNTHESIS AND THERMOELECTRIC CHARACTERIZATION OF $Ca_3Co_4O_9$ PARTICLES

A THESIS SUBMITTED TO
THE GRADUATE SCHOOL OF NATURAL AND APPLIED SCIENCES
OF
MIDDLE EAST TECHNICAL UNIVERSITY

BY

HEDİYE MERVE ERTUĞRUL

IN PARTIAL FULFILLMENT OF THE REQUIREMENTS
FOR
THE DEGREE OF MASTER OF SCIENCE
IN
METALLURGICAL AND MATERIALS ENGINEERING

AUGUST 2018

Approval of the thesis:

SYNTHESIS AND THERMOELECTRIC CHARACTERIZATION OF

$Ca_3Co_4O_9$ PARTICLES

Submitted by **HEDİYE MERVE ERTUĞRUL** in partial fulfillment of the requirements for the degree of **Master of Science in Metallurgical and Materials Engineering Department, Middle East Technical University** by,

Prof. Dr. Halil Kalıpçılar
Dean, Graduate School of **Natural and Applied Sciences**

Prof. Dr. Cemil Hakan Gür
Head of Department, **Metallurgical and Materials Eng., METU**

Prof. Dr. Ahmet Macit Özenbaş
Supervisor, **Metallurgical and Materials Eng., METU**

Examining Committee Members:

Prof. Dr. M. Vedat Akdeniz
Metallurgical and Materials Eng. Dept., METU

Prof. Dr. Ahmet Macit Özenbaş
Metallurgical and Materials Eng. Dept., METU

Prof. Dr. Amdulla Mekhrabov
Metallurgical and Materials Eng. Dept., METU

Prof. Dr. Kadri Aydınol
Metallurgical and Materials Eng. Dept., METU

Asst. Prof. Dr. Kazım Tur
Metallurgical and Materials Eng. Dept., Atılım University

Date:

I hereby declare that all information in this document has been obtained and presented in accordance with academic rules and ethical conduct. I also declare that, as required by these rules and conduct, I have fully cited and referenced all material and results that are not original to this work.

Name, Last Name: Hediye Merve Ertuğrul

Signature:

ABSTRACT

SYNTHESIS AND THERMOELECTRIC CHARACTERIZATION OF $Ca_3Co_4O_9$ PARTICLES

Ertuğrul, Hediye Merve

M. S., Department of Metallurgical and Materials Engineering

Supervisor: Prof. Dr. A. Macit Özenbaş

August 2018, 71 pages

Thermoelectric materials can convert waste heat to electrical energy as well as thermal energy to electrical energy. Thermoelectric technology can aid to solve the energy problem which causes global environmental problems as an alternative energy source and provide long-lasting power sources which can be used for space missions. $Ca_3Co_4O_9$ is environment friendly, nontoxic, humidity resistant at high temperatures, oxidation resistant, abundant, chemically and thermally stable in air and light. Also, this material is favored because of its natural layered structure which provides high ZT value. Ultrasonic spray pyrolysis method is used for obtaining hollow spherical particles. Thanks to pressure-less sintering method, high amount of porosity in the pellets can be achieved. The aim of this study is that increasing power factor and decreasing thermal conductivity simultaneously through hollow spherical $Ca_3Co_4O_9$ and air composite materials. Hollow spherical particles which are filled with air having low thermal conductivity and the surface of particles which is about 2D and compose of nanoscale constituents provide low thermal conductivity and high power factor.

The powders will be characterized using X-ray diffraction, scanning electron microscopy (SEM), energy dispersive x-ray analysis (EDX) and particle size analysis for structural analysis.

The temperature dependence of Seebeck coefficient and electrical resistivity will be measured using a lab-made system set up in our laboratory in the temperature interval from 300 K to 900 K.

Keywords: Thermoelectrics, $Ca_3Co_4O_9$, Hollow Spherical Particles, Ultrasonic Spray Pyrolysis

ÖZ

$Ca_3Co_4O_9$ PARÇACIKLARIN SENTEZLENMESİ VE TERMOELEKTRİK KARAKTERİZASYONU

Ertuğrul, Hediye Merve

Yüksek Lisans, Metalurji ve Malzeme Mühendisliği

Tez Yöneticisi: Prof. Dr. A. Macit Özenbaş

Ağustos 2018, 71 sayfa

Termoelektrik malzemeler ısı enerjisini elektrik enerjisine çevirebildiği gibi elektrik enerjisini de ısı enerjisine çevirebilmektedir. Termoelektrik teknolojisi global çevre problemlerine neden olan enerji problemlerinin çözümü olabilir ya da uzay görevlerinde uzun ömürlü güç kaynağı olarak kullanılabilir. $Ca_3Co_4O_9$ çevre dostu olması, toksik olmaması, yüksek sıcaklıklarda neme dirençli olması, oksitlenme direncinin yüksek olması, doğada bol miktarda bulunması, kimyasal ve termal olarak kararlı olması ve hafif olması sebepleriyle tercih edilmiştir. Ayrıca bu malzeme doğal katmanlı yapısı sayesinde yüksek ZT değerine sahiptir.

İçi boş küre şeklinde parçacıklar elde etmek için üretim yöntemi olarak ultrasonik sprey piroliz seçilmiştir. Peletlerin basınçsız sinterleme metoduyla üretilmesi sayesinde bol gözenekli bir yapı elde edilmiştir. Bu çalışmanın amacı içi boş küre şeklindeki $Ca_3Co_4O_9$ parçacıklarla güç katsayısını arttırırken termal iletkenliği de düşürmektir. İçi termal iletkenliği çok düşük olan havayla dolu küre şeklindeki parçacıklar ve bu parçacıkların yaklaşık 2D ve nanoölçekli bileşenlerden oluşan yüzeyi sayesinde düşük termal iletkenlik ve yüksek güç katsayısı elde edilir.

Tozların yüzey analizi için XRD, SEM, EDX ve parçacık boyutu analizi yapılmıştır. Termoelektrik özelliklerinin analizi içinse sıcaklığa bağlı Seebeck katsayısı ve elektrik iletkenliği 300'le 900 K arasında ölçülecektir.

Anahtar Sözcükler: Termoelektrikler, $Ca_3Co_4O_9$, İçi Boş Küre Parçacıklar, Ultrasonik Sprey Piroliz

To My Dear Family

ACKNOWLEDGEMENTS

Firstly, I would like to express my appreciation and gratitude to my supervisor Prof. Dr. A. Macit Özenbaş for his support, guidance and patience throughout my study.

I am very grateful to my labmate Kerem Çağatay İçli, Çağrı Özdilek, Başar Süer, Burak Yurdakul, Bahadır Can Kocaoğlu and Mustafa Burak Coşar for their friendship and their support.

My dear friends Damla Dağıstanlı, Bahar Akdeniz, Nadide Aybar, Ece Ferizoğlu, Çiğdem Doğru, Emine Arıkan, Dilek Sezer, Mehmet Can Zeybek, Berna Öztürk, Gülüzar Köysüren, Tuğba Nayır, Beyhan Yılmaz, Dilara Muş, Erol Can Akdoğan, Alican Erdoğan, Sevim Gürkaş, Meltem Özdemir, Uğur Şahan, Özge Ataseven and Merve Doğu have always motivated and supported me in every case. That is why, I will always feel sincere gratitude towards them.

I would like to give special thanks to Ezgi Yavuz who has always supported and encouraged me.

Last but not the least, I would like to thank my family Hamit Ertuğrul, Birsen Ertuğrul Zeynep Melis Ertuğrul, Hayriye Kırkoyun Uysal, Feriha Kırkoyun and Hediye Ertuğrul for their endless support, unconditional love throughout not only this study but also my whole life. I know how lucky I am because I have such a good family and friends.

TABLE OF CONTENTS

LIST OF TABLES

TABLES

LIST OF FIGURES

FIGURES

CHAPTER 1

INTRODUCTION

Reducing fossil fuel utilization and greenhouse gas emission, preventing ozone depletion and providing clean energy are some of the solutions to solve global environmental problems. Thermoelectric (TE) devices that are alternative energy sources can play an important role to solve the energy problem of the world and enable a better future with sustainable energy by converting waste heat into electricity as well as electrical energy into thermal energy. Subjected to a temperature gradient between two ends of the TE material leads to power generation, while cooling or heating is obtained by applying electrical current.

TE materials are used broadly in different areas such as thermal cycles that are for DNA synthesizers, automotive, cooler/heaters for car seat, power generators with low-wattage, applications of personal climate-control, coolers with laser diode and space power generation as these materials are high reliable, not emitting greenhouse gasses, simple, run silently, and practicable for miniaturization. Also, these materials that do not consist of any moving parts and do not use fluids environmentally hazardous have a potential to use for heat pumps or refrigerators. Some sort of radioisotope heat-powered thermoelectric generator have been used for almost whole space probes which are sent beyond Mars because they use waste heat in order to produce electrical energy by radioactive decay. Some of these materials can work more than twenty years and it shows the reliability and stability of these probes [1-3].

To define the efficiency of thermoelectric materials, the dimensionless figure of merit, ZT, is used. The definition of this parameter is,

$$ZT = \frac{S^2 T}{\rho\kappa} = \frac{\alpha^2 T}{\rho(\kappa_L + \kappa_e)} = \frac{PF}{\kappa} \qquad (1)$$

where S is the Seebeck coefficient, T is the temperature, ρ is the electrical resistivity, κ is the thermal conductivity which is equal to sum of κ_L lattice (phonon and magnon) thermal conductivity and κ_e charge-carrier thermal conductivity and PF is the power factor [3].

To obtain high efficient TE materials, ZT value should be high insofar as possible. High Seebeck coefficient, low electrical resistivity and low thermal conductivity are required getting high ZT. However, optimization of ZT is very difficult due to the interdependent coefficients (S, ρ, κ). For instance, when the Seebeck coefficient (S) increases, electrical resistivity (ρ) usually increases, too. Also, increasing the electrical conductivity (σ) means rising electronic thermal conductivity (κ_e) according to Wiedemann-Franz law which is defined as [4],

$$\kappa_e = L\sigma T \qquad (2)$$

where L is the Lorenz number. Also, after κ_e is calculated from this formula, κ_L can be obtained by subtracting the κ_e which is electronic thermal conductivity from the κ_{tot} which is the total thermal conductivity [5].

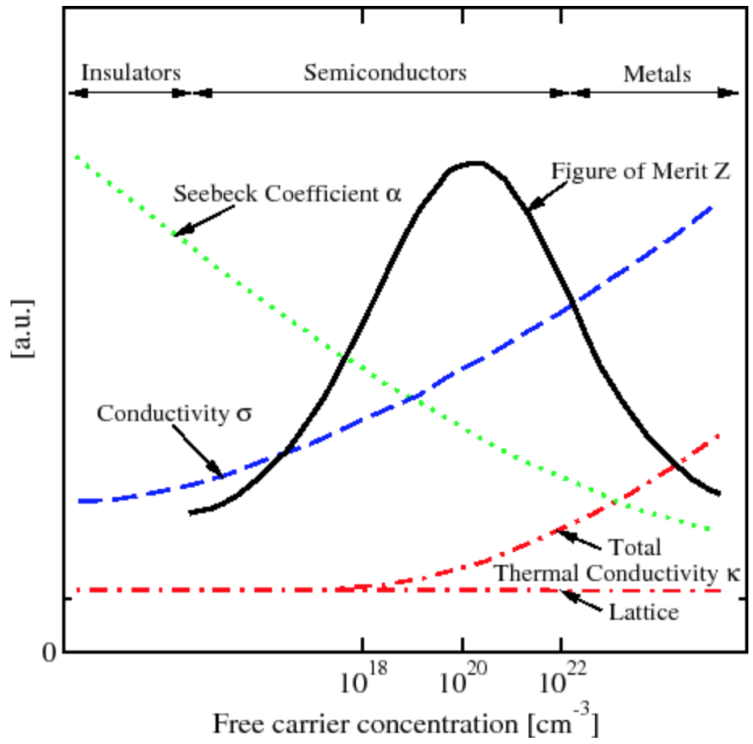

Figure 1. The relation between ZT, Seebeck coefficient, thermal conductivity, conductivity and free carrier concentration [6].

The Seebeck coefficient, thermal conductivity and electrical conductivity depend on one another due to many factors such as carrier concentration, band structure and so on [7]. The effect of carrier concentration on Seebeck coefficient, thermal conductivity, electrical conductivity and ZT is indicated by Figure 1 [6].

For current materials, ZT is around 1, but this value is insufficient for widespread applications [8]. According to the researches, if ZT equals to 4, thermoelectric refrigerators which are used in home can compete with conventional compressor-based refrigerators economically. Even so, more modest rise in ZT can substantially affect applications of thermoelectric materials [9]. The definition of conversion efficiency is,

$$\eta = \eta_c \frac{\sqrt{1+ZT}-1}{\sqrt{1+ZT}+T_c/T_h} \qquad (3)$$

where η, T_c, T_h and η_c are conversion efficiency of heat energy to electrical energy, the temperature of cold side, the temperature of hot side and Carnot efficiency which is defined as $\eta_c = 1 - T_c/T_h$, respectively [10]. Figure 2 shows that the relation between he conversion efficiency and ZT. According to this figure, ZT values of thermoelectric materials should be above 3 due to being in competition with traditional power generators that can achieve 40% of Carnot efficiency [10].

Although there are many researches about promising oxide-based materials such as In_2O_3-based materials having ZT ~ 0.45 at 973 K, $Ca_3Co_4O_9$-based materials having ZT ~ 0.35 at 1000 K and $CaMnO_3$-based materials having ZT ~ 0.25 at 973 K over the past few decades, these ZT values are insufficient yet because this situation causes limitations of the applications of TE oxides as it can be seen in Figure 2 [11].

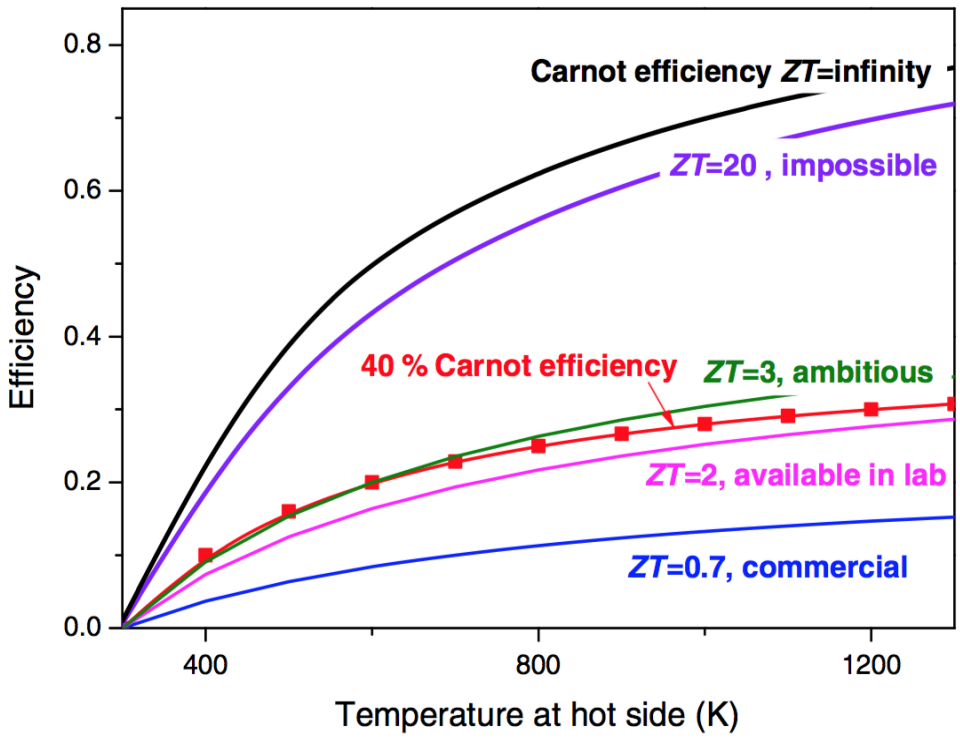

Figure 2. Conversion efficiency of TE materials with changing temperature difference and ZT, assuming that the cold side temperature is 300 K [10].

There are lots of approaches to increase ZT in the field of thermoelectricity such as all-scale hierarchical architecturing in order to decrease the lattice thermal conductivity, altering the band structure, electron energy barrier filtering in order to increase Seebeck coefficients, band convergence, quantum confinement effects and nanostructuring. The aim of majority of these approaches is to maintain a high power factor and/or reduce the lattice thermal conductivity [12]. In the view of such information, in this study, enhancing power factor and reducing thermal conductivity are aimed simultaneously by producing hollow spherical $Ca_3Co_4O_9$ and air composite materials. High power factor and low thermal conductivity can be obtained at the same time by hollow spherical particles which are filled with air, having surface of particles about 2D, and having particles consisting of nanoscale constituents. Also, porosity is very high in the matrix of materials thanks to pressure-less sintering method.

CHAPTER 2

LITERATURE SURVEY

2.1 Application Areas of Thermoelectric Materials

Nowadays, thanks to their marked advantages such as having high stability, having portable weight, needing no maintenance, being environmentally friendly, being reliable, operating in silence and needing no mechanical movement thermoelectric materials draw attention in the usage areas of thermal sensors, power generators, coolers and heat pumps [10,13]. The prerequisites of using a thermoelectric material in industrial applications are not only having a large figure of merit but also the properties of materials such as producing with synthesis method which is as easy as possible, easily scalable, not necessary long thermal treatments if they have to produce under a protective atmosphere [14].

The application areas of thermoelectric materials are so widely such as power generating clothing to utilize harvest body temperature energy [15], health monitoring that is self-powered [16], radioisotope thermoelectric generators for the deep-space applications like NASA's Voyager and Cassini and power generations for automotive industry [17]. For instance, when TE materials are used for electrical generators, the waste heat which is released in engine combustion is tapped by TE devices, so TE devices make more effective automobiles [18].

Figure 3 indicates comparison of different thermoelectric materials for utilization of refrigeration and waste heat harvest, in terms of being abundant, temperature interval of process and being environment friendly for constituent elements. In spite of low ZT values of oxide compared with the some other types TE materials, they own many inherent properties for applications. First, oxides can be used for a large temperature gradient thanks to being stable chemically and thermally. Second, due to structural intricacy and chemical versatility of oxides, these materials can offer excellent flexibility of compositional and structural tailoring. Third, the large temperature gradient can bring about some thermoelectric effects which are nonlocal and these can

be favorable thermoelectrically. Finally, the raw materials of oxides are favored because of their low cost and oxide materials are eco-friendly [19].

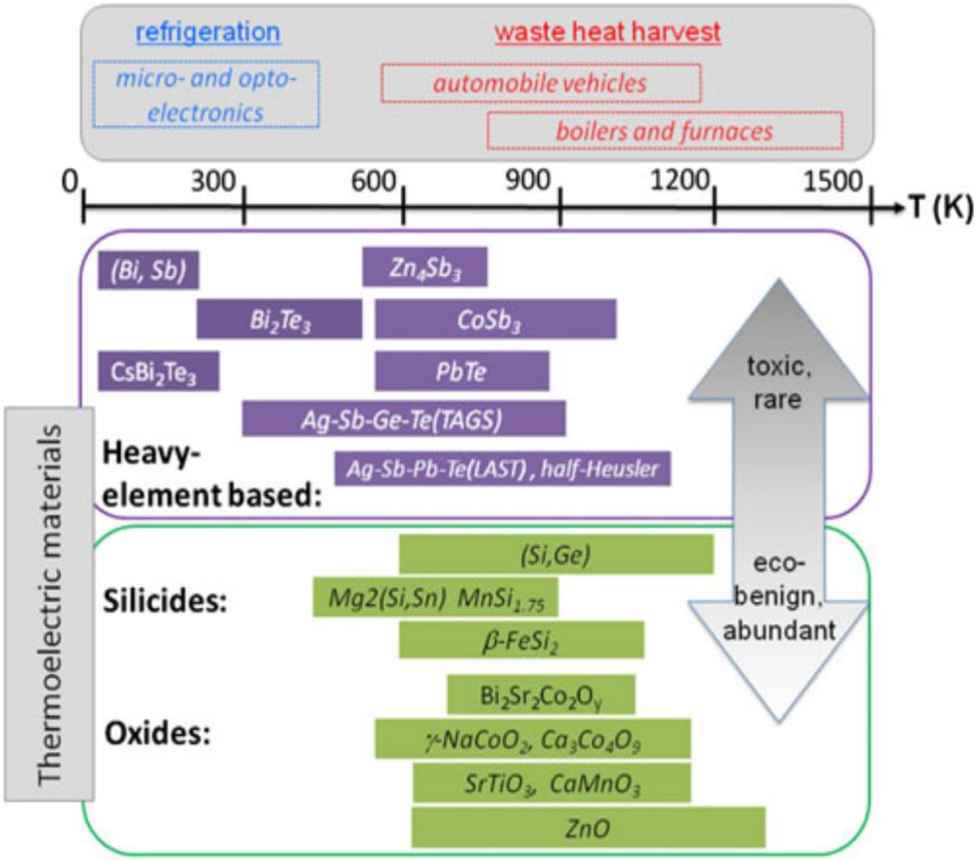

Figure 3. Schematic comparison of different TE materials for utilizations in terms of the operation temperature and being abundant and environment friendly [19].

As it can be seen in Figure 4, PV, CSP, TI, and Org denote photovoltaic, concentrated solar power, thermionic devices and organic devices, respectively. It compares the efficiency of different kinds of energy conversion technologies with TE power generators. In spite of not exciting any theoretical limit for ZT, development of ZT is generally slow and this situation causes limitations for using TE materials in practical applications. In point of fact, the efficiency of TE devices can be compared different renewable technologies like single junction photovoltaic cells when ZT is 1 and temperature differences are considered. Furthermore, since presently above 90% of the energy supply is used as heat and almost 60% of the energy input is waste heat, so lots of available heat sources are fundamentally free to recycle [20].

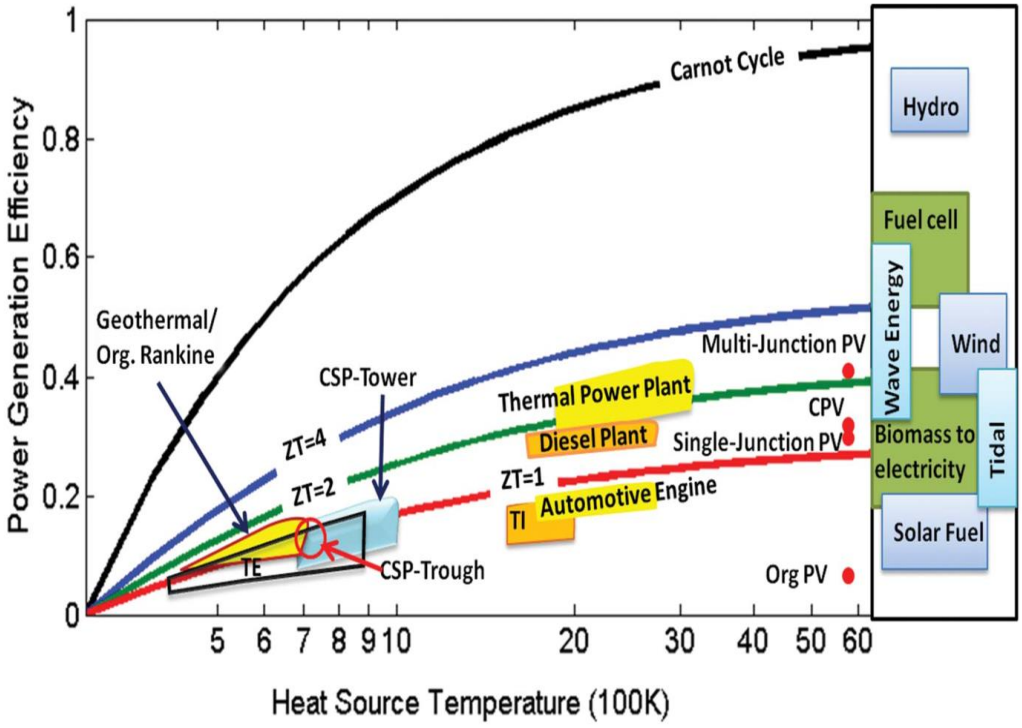

Figure 4. For various energy conversion technologies, power generation efficiency versus the hot side temperature, assuming that the cold side is at room temperature [20].

2.2 Thermoelectric Effects and Theoretical Background

2.2.1 Seebeck Effect

The phenomenon of the transformation of heat energy into electrical energy bases on the Seebeck effect. For appreciation of its physical significance, the outcome of imposing a constant temperature gradient on a finite conductor. The charge carriers distribute homogeneously in the conductor. However, when a temperature gradient is applied, kinetic energy of the free carriers which are at the hot end increases , so these carriers tend to diffuse from the hot end to the cold end. The accumulation of charges brings about a back emf that opposes a further charge flowing. The Seebeck voltage is the open circuit voltage when current does not flow [21].

In order to discuss TE effect that underlie conversion of TE energy, Figure 5 is

examined. Two different conductors which are a and b form a circuit. These conductors are connected electrically in series. On the other hands, they are connected thermally in parallel. If the A and B points which are junctions have dissimilar temperatures that are T_1 and T_2 and $T_1 > T_2$, V occurs between C and D. V is defined as [22],

$$V = S(T_1 - T_2) \qquad (4)$$

$$S = \frac{V}{\Delta T} \qquad (5)$$

where S, V and ΔT are differential Seebeck coefficient between the a and b elements, an open circuit potential difference and temperature difference, respectively.

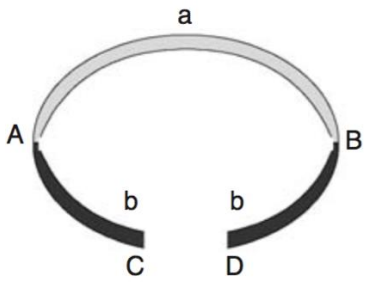

Figure 5. The scheme of basic thermocouple [22].

If there is small temperature differences, the relationship of between V and ΔT is linear. When the emf leads to a current which flows in a clockwise direction around the circuit, the sign of Seebeck coefficient is positive [22]. When the semiconductor is n-type, the Seebeck coefficient is negative and when the semiconductor is p-type, the Seebeck coefficient is positive [21]. Hence, the choice of materials affects the sign and magnitude of S [21]. One of the popular application of the Seebeck effect is measurement of temperature via thermocouple [23].

2.2.2 Peltier Effect

The complementary effect of the Seebeck effect is the Peltier effect. Thermoelectric refrigeration is based on this phenomenon [21]. When there is a current which pass though the junctions of two different materials, a temperature difference take places. For the Peltier effect, heat Q is absorbed at one junction and liberated at the other junction.

Definition of the Peltier effect is [23],

$$\pi_{ab} = \frac{Q}{I} \qquad (6)$$

where π_{ab}, Q and I are the Peltier coefficient, absorbed heat and current, respectively. By convention, the sign of π_{ab} is positive if current flows from a to b and the surroundings absorbs Q [21].

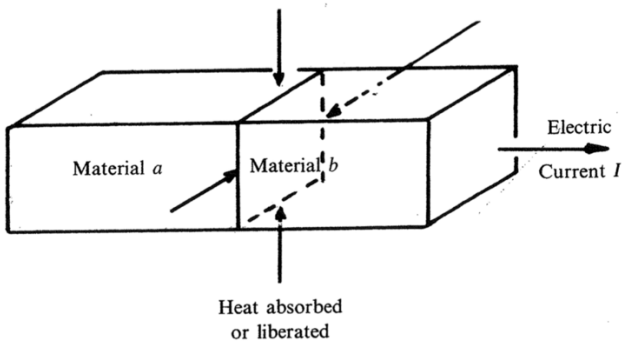

Figure 6. The scheme of Peltier effect [21].

There is a relation between the Seebeck and Peltier coefficients which is defined as [23],

$$\pi = ST = \frac{Q}{I} \qquad (7)$$

2.2.3 Thomson Effect

When a gradient of temperature and an electric current exist at the same time, the Thomson effect appears. When a material is submitted to a gradient of temperature and a current passes through this material, heat is exchanged with the outside medium by the material. Conversely, when a material is submitted to a temperature gradient and a heat flux passes through the material, a current is generated [23]. Definition of the Thomson effect is,

$$Q = \beta I \Delta T \qquad (8)$$

where Q, β, I and ΔT are the rate of reversible heat, the Thomson coefficient and temperature difference, respectively [21].

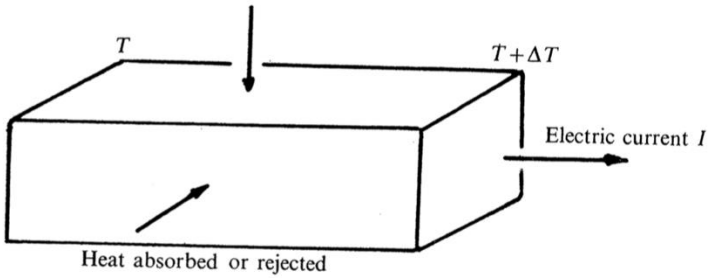

Figure 7. The scheme of Thomson effect [21].

The kelvin relationships relate the three thermoelectric coefficients which are [21],

$$S_{ab} = \frac{\pi_{ab}}{T} \quad \text{and} \quad \frac{dS_{ab}}{dT} = \frac{\beta_a - \beta_b}{T} \qquad (9)$$

2.2.4 Thermoelectric Modules and Power Conversion Efficiency

Two dissimilar conducting materials which contain positive charge carriers which are holes and negative charge carriers which are electrons form a junction in a typical thermoelectric device.

Positive and negative charge carriers move off from the junction and transmit heat when an electric current is moved through the junction. Likewise, when heat source is put at the junction, carriers flow away from there and electric is generated. One of the advantages of these materials does not need any moving parts. Also, these materials are low-cost, lightweight and they wholly get rid of the use of chloroflurocarbons or hydrochloroflurocarbon which are bulk fluids [18].

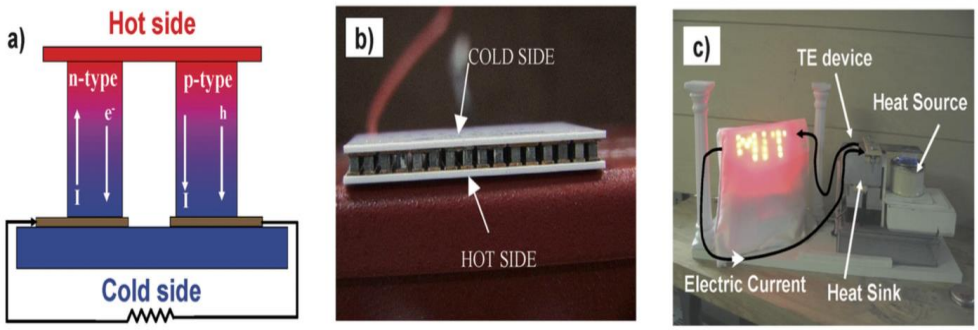

Figure 8. (a) The scheme of thermoelectric power generation (b) a typical thermoelectric module (c) a performance of thermoelectric power generation [2].

The coefficient of performance (COP) expresses the capability of a refrigerator. To define the COP, the cooling amount is divided by the input of electrical energy which is necessary obtaining that cooling. According to the thermodynamics laws, Carnot efficiency which is a maximum efficiency cannot be overgrown. The COP is defined as $T_{cold}/(T_{hot}-T_{cold})$ at Carnot efficiency where T_{hot} is temperature of the ambient environment and T_{cold} is temperature of the coolest part which is in the refrigerator [18].

Connecting two doped semiconductive materials which are n-type and p-type constitute TE cooler which is shown in Figure 9-A. If a current moves from the material that is n-type to the material that is p-type, the dominant carriers which are holes or electrons of materials move off from the junction and transport heat. The junction get cold because heat is moved away from the junction by the electrical current. This effect is Peltier effect. This device can also be used for generation of electricity which is shown in Figure 9-B when the junction is purposely heated.

For this case, the current of the electrical carriers partly transport the heat from junction to the bottom and it produces a voltage between the ends of the TE couple [18].

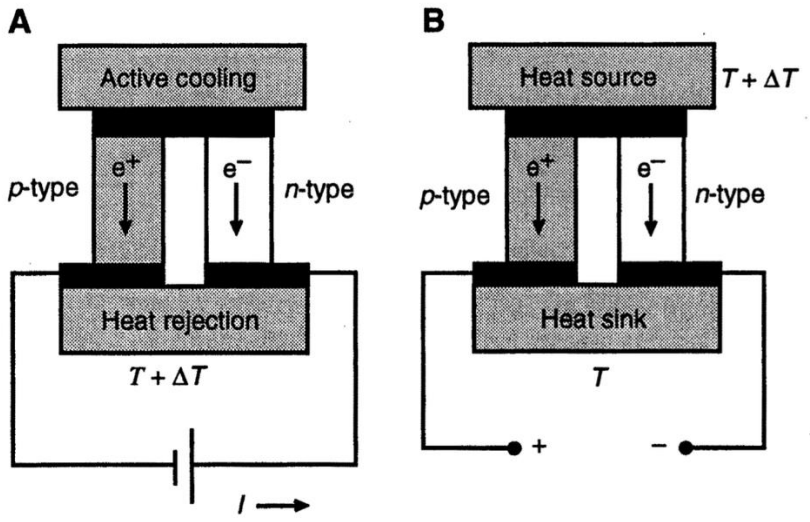

Figure 9. The schemes of TE couples [18].

2.3 Methods For Enhancement of Figure of Merit (ZT)

Obtaining thermoelectric materials having high ZT can be provided by increase in the power factor or decrease in the thermal conductivity. They can be achieved by many techniques such as nanoscale dots [24], synthesizing parent nanocrystals [25], synthesizing a crystalline structure having low thermal conductivity via increasing scatter of phonon at the interfaces, having heavy elements and presence of weak bonds between layers [20], electron energy barrier filtering [26], ions doping [27], designing materials which contains natural superlattices [28], modifying the band structure by electronic resonance states [29] and designing quantum confinement effects [30].

2.3.1 Nanostructuring Approach

For bulk three-dimensional materials, transport features of nano-structures and micro-structures are different. The nano-structures' thermal conductivity is weaker than the

thermal conductivity of bulk materials. This is advantage of nano-structures for thermoelectric properties. On the other hand, the manufacturing methods of nanostructured materials is generally thin films techniques such as pulsed laser, molecular beam epitaxy, CVD and so on which are too expensive for large scale productions [23].

The reasons of obtained high figure of merit by nanostructured materials are the enhanced carrier density of states and the reduction of thermal conductivity because of the phonon spectrum modification or phonon–boundary scattering [22].

A significant decrease in κ is achieved by nanostructuring which provides the high grain boundary density and scattering of phonons are stronger selective than scattering of charge carriers [31].

2.3.2 Low-Dimensional Structures

Obtaining high ZT value can be achieved by many techniques and one of them is using low dimensional structures which provides the increment of Seebeck coefficient because low dimensional structures lead to quantum confinement effect. There is strong relationship between dimensionality and electronic DOS [32].

Effect of dimensionality on the band structure can modify the electronic transport properties. For 3D material, S, ρ and κ are interdependent so optimizing these parameters is so difficult. On the other hand, for low dimensional materials, these parameters can become independent [23]. Also, reducing dimensions may lead to a decrease in the lattice conductivity [22].

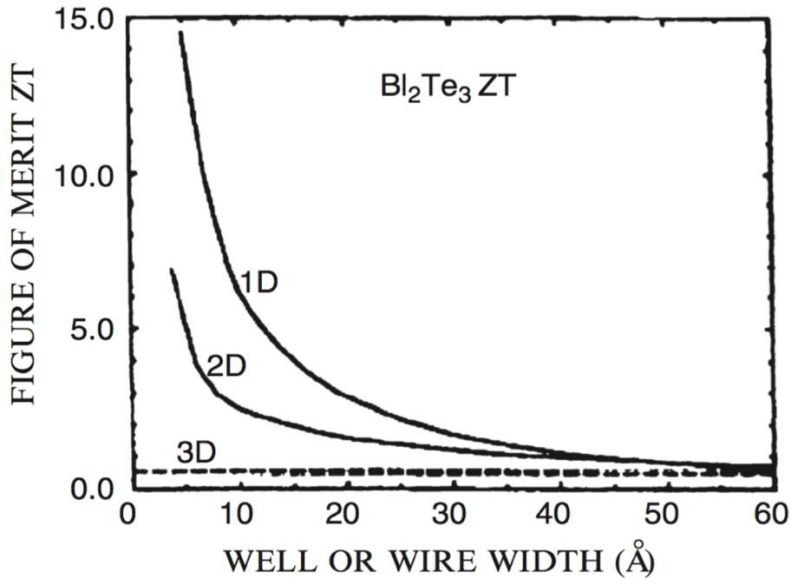

Figure 10. Changing ZT with respect to the dimensionality [23].

It is incredible that before the some experimental observation, the enhancement of ZT has been predicted in theory as shown in Figure 10 [23].

2.3.3 Grain Size Effect

Generally, the thermal conductivity of the crystal lattice has a mainly effect on the thermal conductivity and the thermal conductivity of the crystal lattice depends on the transport of phonon in the crystal lattice. It can be restricted by phonon scattering that can be achieved by boundaries of crystal and point defects [9]. On the other hand, electrical conductivity of samples having smaller particle size is very low because of the increasing scatter of charge carriers by the enhanced density of grain boundaries, so increasing particle size brings about increasing electrical conductivity [31].

When the grain size of materials is reduced moderately like from a few μm to about 300 nm, this leads to reduce lattice thermal conductivity due to scattering of phonons which have long wavelength while the electrical conductivity does not change [33].

2.3.4 Doping

According to the researches, doped $CoSb_3$, filled $CoSb_3$, and inclusion dispersed $CoSb_3$ are searched in order to decrease the thermal conductivity [34].

This method which is doping is used to develop the properties of electrical transport by enhancing the carrier concentration. Also, another approach is enhancing carrier mobility [11]. Seebeck coefficient can be improved by simple doping of impurities due to changing the electron DOS which is shown as,

$$S = \frac{8\pi^2 k_B^2}{3eh^2} m^* T \left(\frac{\pi}{3n}\right)^{2/3} \qquad (10)$$

where, m^*, k_B, n, h are effective mass of the charge carriers, Boltzmann constant, the density of charge carriers and Planck constant, respectively. The carrier concentration and m^* mainly control the Seebeck coefficient [10].

On the other hand, doping causes decrease in Seebeck coefficient of the highly degenerate semiconductors due to Pisarenko relationship which is S œ $n^{-2/3}$, where the carrier concentration is n [35].

Li et al. demonstrated that when Na content scales up, the total thermal conductivity scales up, too because of the increased electrical thermal conductivity. Also, when Na content increases, the lattice thermal conductivity reduces slightly due to scattering of point defect which occurs because of the size and the difference between the atom mass of Ba and Na [36].

The aim of many researches is increased ZT value of $Ca_3Co_4O_9$ which is polycrystalline by doping approach. The major challenge of this aim is studying out a dopant that enhance Seebeck coefficient and electrical conductivity of material and decrease thermal conductivity of it, simultaneously [37]. The effects of different dopants is shown in Figure 11. According to Saini et al. [37], Terbium provides highest ZT value for doped $Ca_3Co_4O_9$.

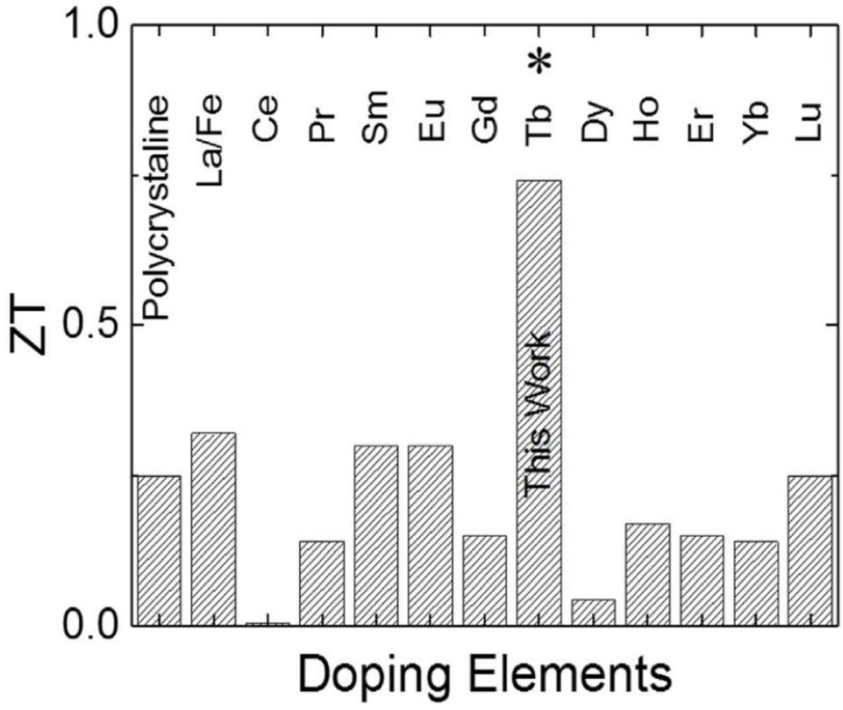

Figure 11. ZT of various rare earth doped C349 samples [37].

2.4 Thermoelectric Materials

Thermoelectric materials are classified into two categories which are oxide-based materials and metallic alloys. The materials that are alloy-based possess high ZT value such as PbTe and Bi_2Te_3 that are typical examples and other systems such as skutterudites. In spite of high ZT value of them, these materials are expensive, toxic, having phase transition, thermally unstable at elevated temperatures. To eliminate these issues, oxide-based materials such as simple oxides, layered oxide-based materials and perovskite-like materials are researched [38].

2.4.1 Oxide Based Thermoelectric Materials

Metal oxides which are chemically, structurally and thermally stable in air, have high oxidation resistance, are produced easily, have low cost and are environment friendly are more favorable than the conventional thermoelectric alloys at high temperatures.

Nonetheless, the powerful ionic feature and strong carrier scattering due to the large difference between electronegativity of constituent elements commonly leads to localization of electrons which have low carrier mobilities. It means that property of electrical transport is poor. Also, thermal conductivity of them is relatively high because of simple crystal structure, high bond energy and airy constituting elements that causes poor phonon scattering of metal oxides. For these reason, TE performance of metal oxide is more inadequate than TE performance of traditional thermoelectric alloys. However, some of the transition metal oxides such as cobaltites, manganites and titanates that possess some properties to increase ZT have discovered. One of them is misfit-layered $Ca_3Co_4O_9$ whose structure is natural superlattice presents unusual thermoelectric features having a low electrical resistivity and a high thermopower, simultaneously [27,39].

Oxide-based thermoelectric materials are favored research subject due to having inherently low thermal conductivity [40]. Also, they are ecologically friendly and present high figure of merit [37].

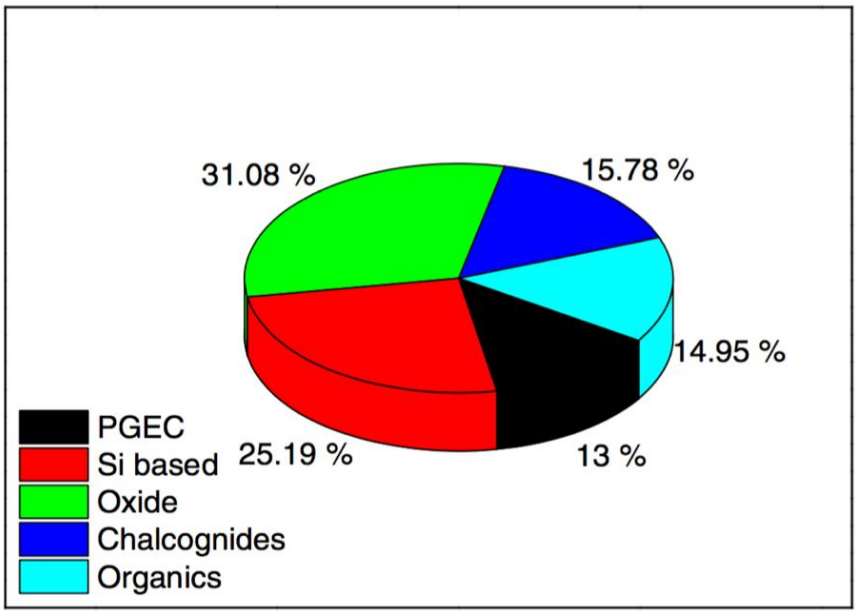

Figure 12. Schematic comparison of different sorts of thermoelectric materials from 2010 to 2013 [10].

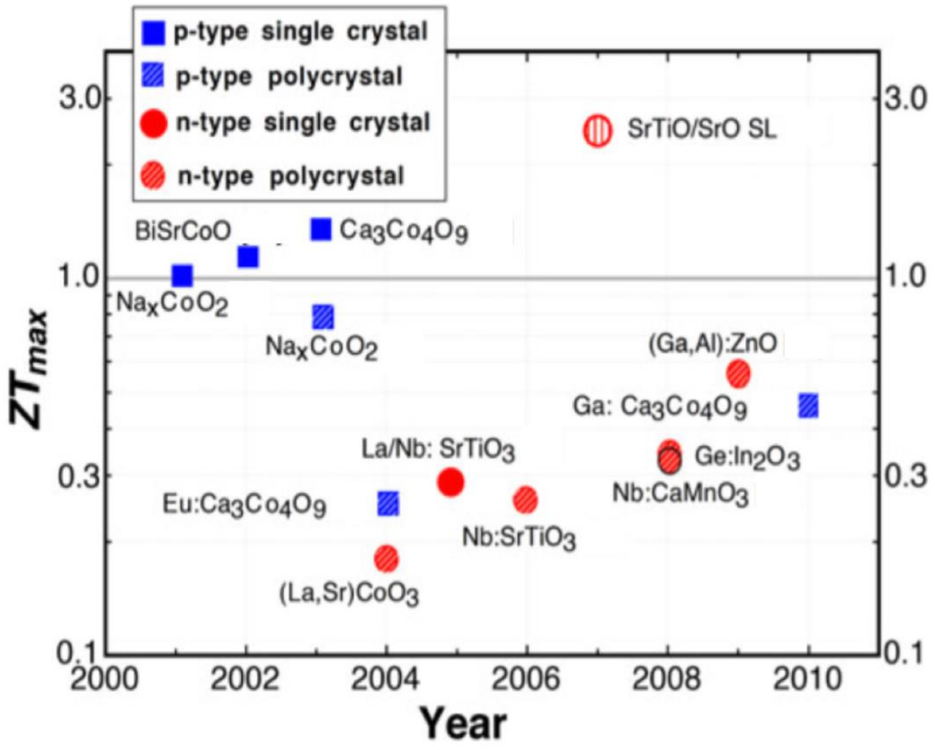

Figure 13. The timeline of the maximum ZT of p-type and n-type TE oxides [19].

2.4.2 $Ca_3Co_4O_9$ Oxide Thermoelectric Materials

One of the best thermoelectric oxides that are p-type is misfit layered $Ca_3Co_4O_{9+\delta}$ when it is compared with other oxides [41]. Calcium cobaltite is light, nontoxic, not having polluting character, abundant, having low cost, oxidation resistant, thermally and chemically stable in air and humidity resistant at elevated temperatures [41-45]. $Ca_3Co_4O_9$ can be used for many applications such as a hydrogen evolution catalyst, a transparent conducting oxide and material of electrode in fuel cells [43].

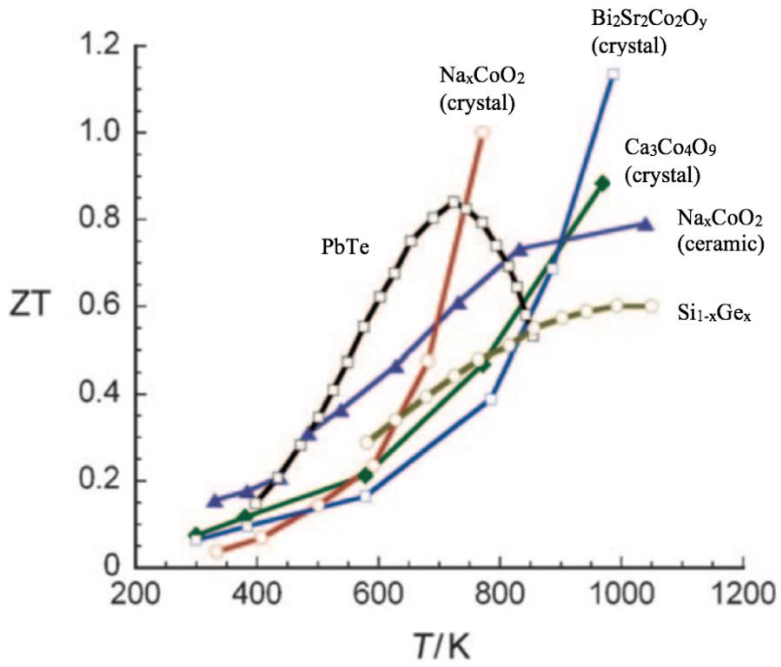

Figure 14. ZT values of some favourable oxides versus temperature [46].

The best figure of merit values of p-type oxides are shown in Figure 14 [46].

One of the main challenges about TE materials is to discover a TE material that is stable and have ZT value about 1. In despite of existing of such materials whose ZT is about 1, applications of them are limited because of issues about being stable chemically and toxicity [37].

To achieve high ZT value, both high power factor and low thermal conductivity are required but these parameters are contradictory. Infrequent materials possess some properties to break relationship between these parameters. One of these materials is layered cobalt oxides [37].

In order to produce a suitable thermoelectric modules used at high temperature (larger than 573 K), the essential properties are good thermal stability to prevent decomposition, evaporation or oxidation during long duration in the temperature interval of the utilization, not displaying structural phase transitions that can be unfavorable for thermal cycle or ionic conductance [47].

Layered Cobalt oxides materials which are p-type draw attention for the application areas of thermoelectric materials. The reason of this is crystal structure of them. There are two layers in their crystal structure. One layer has a powerfully correlative electron system which provides an electronic transport way and the other layer provides a region of phonon scattering [40].

To develop performance of the thermoelectric materials, materials which have natural superlattices are designed. These materials possess layers. When one of the layers provides perfect electronic transport features, the other one provides phonon scattering. The example of these properties can be layered cobalt oxides [48].

There are lots of researches about cobaltate with misfit layered ($Ca_3Co_4O_9$) and alternative transition metal oxides due to its structure with natural layered and having powerful anisotropy in TE features of it [49]. This structure can be regarded as natural superlattices that compose of alternately stacked layers of conduction and insulation [50]. $[Ca_2CoO_3]_{0.62}[CoO_2]$ structurally represent $Ca_3Co_4O_9$. Ca_2CoO_3 layers that are rock-salt-type and CoO_2 layers that are CdI_2 type are two subsystems constituting this structure [49]. In $Ca_3Co_4O_9$, CoO_2 conducting layers having a strongly correlated electron system provide layers of electronic transport while misfit layers of Ca_2CoO_3 which is an layer of insulation provide regions of phonon scattering [49, 51]. As shown in Figure 15, along the direction of c-axis, layers of Ca_2CoO_3 and CoO_2 are stacked alternately. Along the direction of c-axis, the a, c and β lattice parameters are same, but along the direction of b-axis, there is a lattice parameter which is different causes a structural mismatch. Therefore, anisotropic behavior is observed for TE transport features of $Ca_3Co_4O_9$ measured vertical and horizontal according to the pressure axis [49].

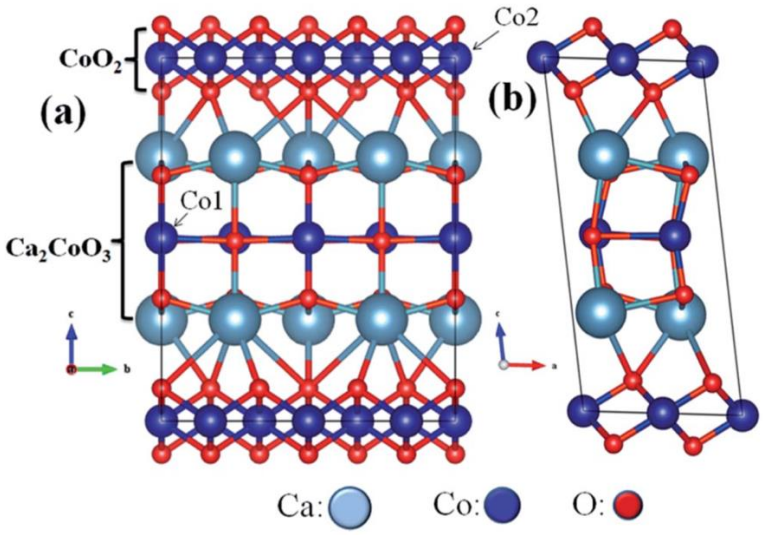

Figure 15. The scheme of the crystal structure of C349 vertical to (a) the a axis (b) the b axis [49].

So many researches has focused on improved ZT value of $Ca_3Co_4O_9$. To achieve this, many techniques are used. In 2016, Schulz et. al. reported that ZT value of $Ca_3Co_4O_9$ fabricated by pressure-less sintering is ~0.06 [52]. In 2017, Saini et al. demonstrated that ZT value, Seebeck coefficient, electrical resistivity and thermal conductivity of $Ca_{2.5}Tb_{0.5}Co_4O_9$ are 0.74, ~323 μV/K, nearly 9 mΩ.cm and ~1.21 W/mK at 800 K, respectively [37]. In 2009, Lin et. al. demonstrated a figure of merit of ~0.18 and ~173 μV/K Seebeck coefficient at 975 K in pure $Ca_3Co_4O_9$ fabricated by spark plasma sintering [53]. Shikano et. al. reported that $Ca_3Co_4O_9$ samples with single crystal have one of the highest ZT value in cobaltites ~0.87 with nearly 240 μV/K Seebeck coefficient, ~3 W/mK thermal conductivity and ~2.3 mΩ.cm electrical resistivity at 973 K [54]. However, $Ca_3Co_4O_9$ samples with single crystal are limited in practical applications because they cannot be manufactured in a large amount because of small sizes of them. Therefore, the purpose of the researches is finding out $Ca_3Co_4O_9$ samples with polycrystal having high ZT values [37,55].

Table 1. TE properties of C349 materials from the literature

Material	Method	T (K)	S (μV/K)	κ (W/mK)	R (mΩ.cm)	PF (μW/mK^2)	ZT	Ref.
C349	Solid state SPS*	1000	177	1.65	8.97	350	0.21	[56]
C349	Mixed-oxide route Pressure-less sintering	873	146	2.5	12.65	170	0.06	[52]
C349	Sol-gel SPS	1000	163	1.67	10.8	295	0.15	[49]
C349	Solid state Hot-pressing	900	175	3.1	6.2	525	0.16	[57]
C349	Solid state Cold-pressing	1073	27	-	30	245	-	[58]
C349	Solid state Cold-pressing	800	170	-	42	80	-	[59]
C349	Pulsed laser deposition	823	192	-	7.1	520	-	[60]
CC0**	Sol-gel SPS	973	164	-	5.71	-	-	[61]
C349	Ball milling Hot-pressing	900	172	3.1	8.2	555	0.16	[44]

* SPS is the spark plasma sintering.

** $(Ca_{0.9}La_{0.075}K_{0.025})_3Co_4O_9$

Table 2. TE properties of C349 materials from the literature

Material	Method	T (K)	S (μV/K)	κ (W/mK)	R (mΩ.cm)	PF (μW/mK^2)	ZT	Ref.
CC0*	Sol-gel SPS Dynamic forging	973	155	2.067	4.69	530	0.26	[53]
C349	Sol-gel SPS	973	173	2.1	8.47	351	0.16	[62]
C349	Sol-gel CS**	973	186	2.1	29.41	115	0.052	[62]
CC0*	Sol-gel Cold-pressing	1073	184	1.71	4	815	0.52	[41]
C349	Solid state Cold pressing	293	56	2.5	0.13	2000	-	[63]
C349	LFZ****	1073	205	-	10	420	-	[64]
C349	Cold-pressing	300	133	0.98	15	-	0.035	[65]
CCO******	Solid state Cold-pressing	800	323	1.21	9	1150	0.74	[37]
C349	Modified strontium chloride flux technique	973	240	3	2.3	-	0.87	[54]

* $(La_{0.1}Ca_{0.9})_3Co_4O_9$

** CS is the conventional sintering.

*** $Ca_3Ba_{0.05}Co_4O_{9+\delta}$

**** LFZ is laser floating zone technique.

***** $Ca_{3-x}Tb_xCo_4O_9$, x = 0.5

2.5 Production Methods of Thermoelectric Materials

There are many fabrication methods to manufacture thermoelectric materials such as HP which is hot-pressing, SPS which is spark plasma sintering, solid state reaction, sol-gel and so on [55,66]. Ultrasonic spray pyrolysis (USP) is chosen method for generation of hollow spherical $Ca_3Co_4O_9$ particles. Nanopowder and nanostructured material production methods provide control on economy, phase composition, productivity and dispersity [67]. There are lots of parameters such as the temperature of reactor, the ultrasonic generator frequency, the chemical compound, the atmosphere in the reactor, the rate of flow of the carrier gas, and the concentration of initial solution having significant influence on the structure, dispersity, the phase composition and morphology of the end product. Thanks to spray pyrolysis method, these parameters can be controlled easily. The formation of hollow microspheres needs the high mass transfer and high rate of evaporation [67]. In spray pyrolysis, atomization of a solution with fine droplets is occurred. Then, these droplets put in a reactor and they dry in there. After these, a chemical reaction takes place and some elements separate from the source material [68].

To obtain aerosol droplets, hydraulic, ultrasonic, pneumatic, mechanic, or electrostatic atomizers can be used. The most popular one is ultrasonic atomizer because of being highly productive, producing aerosol droplets with high dispersity and controlling the particle size easily with frequency of atomizer which adjusts the droplet size and the nanoparticle concentration in the precursor [67,69]. A lower droplet diameter is obtained by electrostatic and ultrasonic atomization methods. To obtain films on a substrate, only the electrostatic method is useful. A higher rate of atomization is achieved by the hydraulic, pneumatic, and mechanic method but the droplets settle down to the initial solution because of a large diameter of the initial droplets having comparatively large mass and being under the influence of the gravity force [67]. The spray method is generally chosen to gain the spherical particles because the particles having spherical shape are generated from the droplets and spherical form is the most stable form for a droplet [70].

Ultrasonic spray pyrolysis method comprises of three distinctly separate periods according to the number of phases in the aerosol droplets. Evaporation is the first period. In this stage, aerosol has the liquid phase completely. The solvent evaporates from the surface of the droplet. The solvent vapors diffuse from the droplet surface to the gas phase.

Then, the droplet shrinks. Temperature changes in the droplet and the solute diffuses toward the center of the droplet. Drying is the second period where solute starts to precipitate on the surface of the droplets. Thermolysis which is the third period starts when the solvent is vaporized wholly. When it takes place, the morphology of particle can transform if the solute can deform [71].

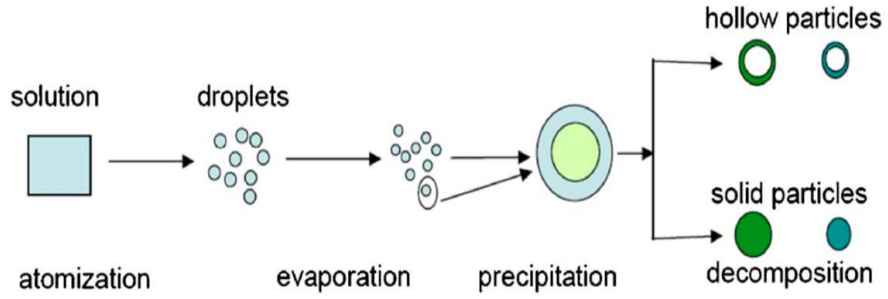

Figure 16. A schematic of the spray pyrolysis technique [68].

Controlling particle morphology has become a very important issue to be considered due to unique chemical and physical properties it provides which are quite different from bulk material itself. These benefits are achieved by the change of shapes of particles. This provides great potential for various applications such as magnetic materials, electronics, sensors, catalysts, pigments, drug carriers, and optical materials, morphological control [70]. If the sprayed droplet dries slowly enough and there is adequate time to redistribute the solute within the droplet due to diffusion throughout the evaporating droplet, the obtained particles are dense dried particles. Conversely, if the sprayed droplet dries fast and there is not enough time for solute in the droplet to diffuse from the surface to the center, hollow particles can be formed [69]. When the solute precipitates only in a thin rigid outer layer and the residual solvent can be taken away without breaking the outer layer, a hollow particle can be formed [71].

The one of the way to get hollow particles is that the vaporization rate is much higher that the solute diffusion rate. When the ambient temperature increases relatively small, reaching to the critical supersaturation concentration of surface is so fast but the solute diffuses too slow to get a uniform concentration for solute, so the concentration of solute at the center of droplet cannot reach to the equilibrium saturation. Moreover, the increasing temperature brings about decrease in the precipitate thickness [71]. Many different precursor solutions can form hollow, shell-like particles because of surface pre- capitation [71].

CHAPTER 3

EXPERIMENTAL STUDIES

In this work, ultrasonic spray pyrolysis (USP) method was used. The precursors dissolved in solution was poured into the ultrasonic generator. The aerosol was formed by collapsing of cavitation bubbles in there and moved through the tube furnace with air by the pump. Then, the obtained powders accumulated at the filter.

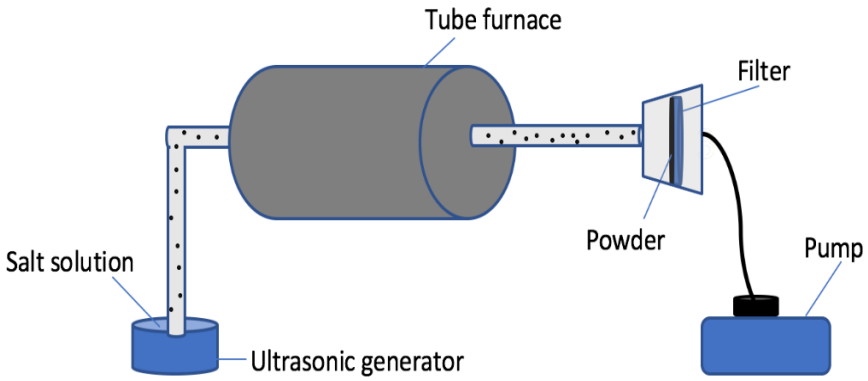

Figure 17. The scheme of ultrasonic spray pyrolysis equipment.

Figure 18. Experimental setup in the laboratory.

3.1 Synthesis of Hollow Spherical $Ca_3Co_4O_9$ Particles

The precursors $Ca(NO_3)_2.4H_2O$ and $Co(NO_3)_2.6H_2O$ were dissolved in three different solutions which were methanol, deionized water and dimethylformamide respectively. These solvents were chosen considering their capability of making aerosol. Temperature of furnace was changed according to the boiling points of solutions. The boiling points of methanol, water and dimethylformamide are 337.7 K, 373 K and 426 K respectively. The solution which was 1.5 M and had methanol solvent was moved into the reactor with a vacuum pump at 923 K. The others which were prepared with deionized water and dimethylformamide and 0.1 M were transferred into the reactor using a vacuum pump at 1173 K. After this process, heat treatment was applied to powders to remove residual salt from them. The parameters of heat treatment were 1123 K during 2 hours. The dimethylformamide is less volatile than water, so phase of $Ca_3Co_4O_9$ could not be obtained with dimethylformamide solution as shown in Figure 19. Getting $Ca_3Co_4O_9$ phase could be achieved by methanol and deionized water solutions. Finally, deionized water was chosen as solvent due to being environment friendly and nontoxic.

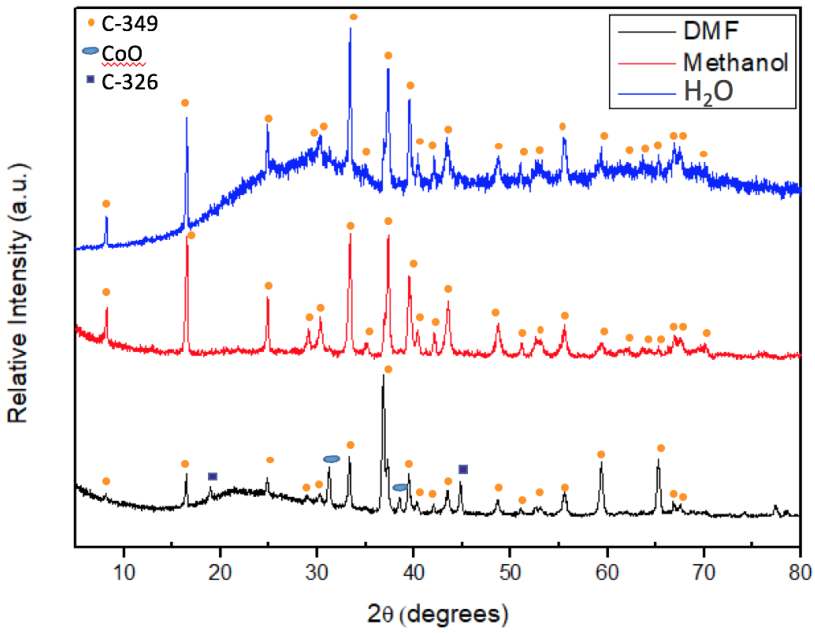

Figure 19. X-ray diffraction pattern of 0.1M C349 sample prepared with methanol, deionized water and dimethylformamide.

After that, the operating temperature of tube furnace was decided. According to X-ray diffraction pattern of $Ca_3Co_4O_9$ sample at 1073 K, 1173 K, 1273 K, 1323 K, 1423 K in tube furnace which are shown in Figure 20 and then having heat treatment at 1123 K during 2 hours, 1173 K was selected as operating temperature of tube furnace due to having $Ca_3Co_4O_9$ phase accomplishedly at this temperature.

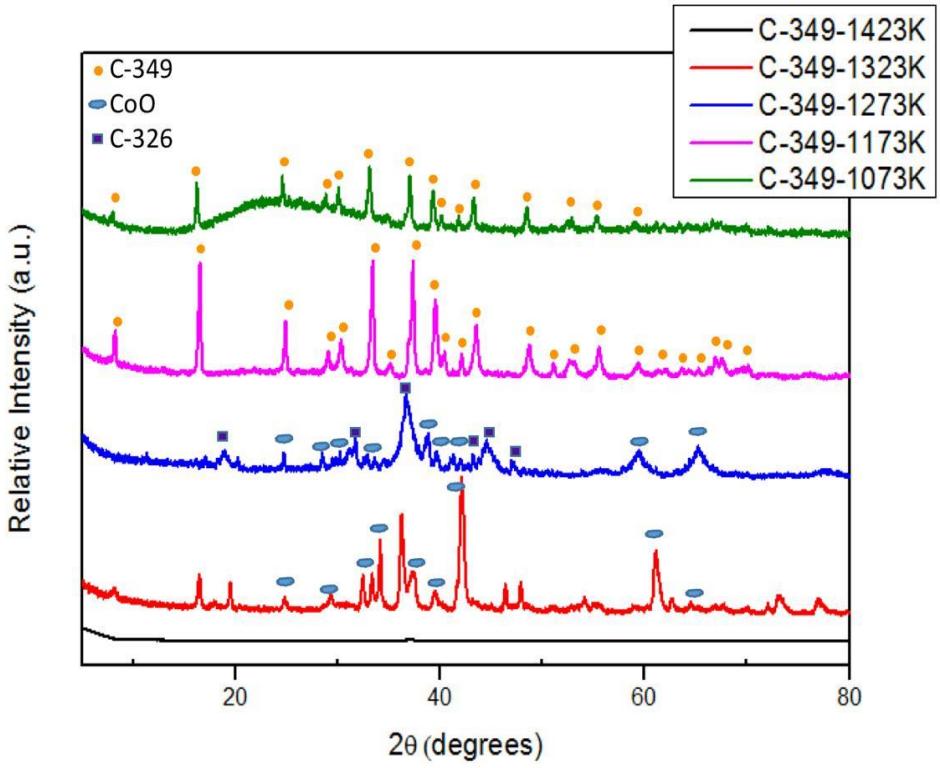

Figure 20. X-ray diffraction pattern of 0.1M C349 sample at 1073, 1173, 1273, 1323, 1423 K in tube furnace and then having heat treatment at 1123 K during 2 hours.

The amount of precursors were determined according to the phase equilibrium diagram of the system CaO-CoO which is shown in Figure 21.

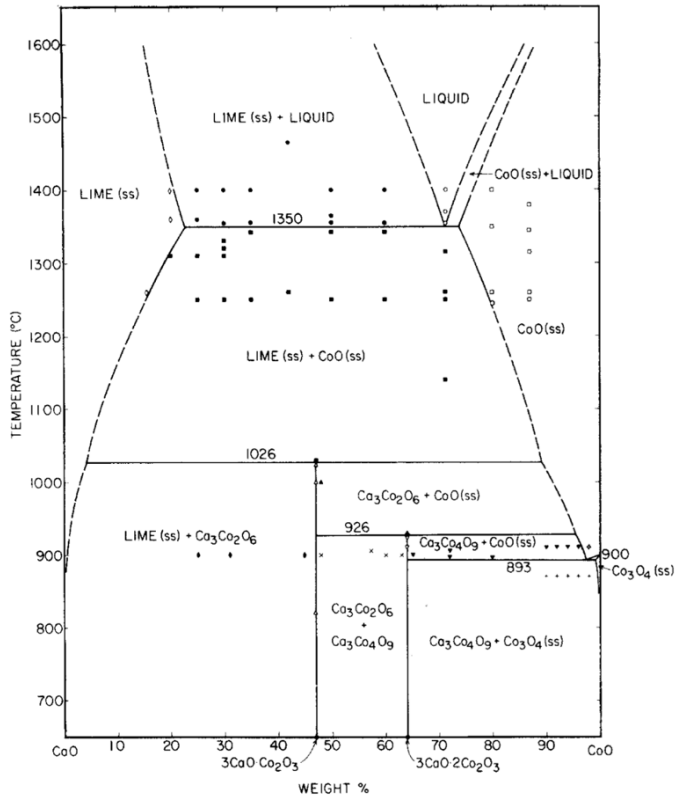

Figure 21. Phase equilibrium diagram for the system CaO-CoO [72].

There are lots of parameters which are the amount of precursors, temperature of furnace and air flow which get through the furnace to influence the final morphology, the structure and the phase composition. To obtain hollow particles, the high-evaporation rate and high-mass transfer are provided. When flow rate is low in the tube furnace, monolithic spherical particles are produced. Conversely, when high flow rate is obtained in the tube furnace, hollow spherical particles are formed [67]. Therefore, getting hollow microspheres, high flow rate in tube furnace and 1173 K as operating temperature of tube furnace are chosen. Thermal drying and thermal decomposition of an aerosol droplet of the solution solved precursors are based of this method. Firstly, evaporation of the droplets and then thermal decomposition happens. As a result, a metal oxide and a nitrogen dioxide are produced [67].

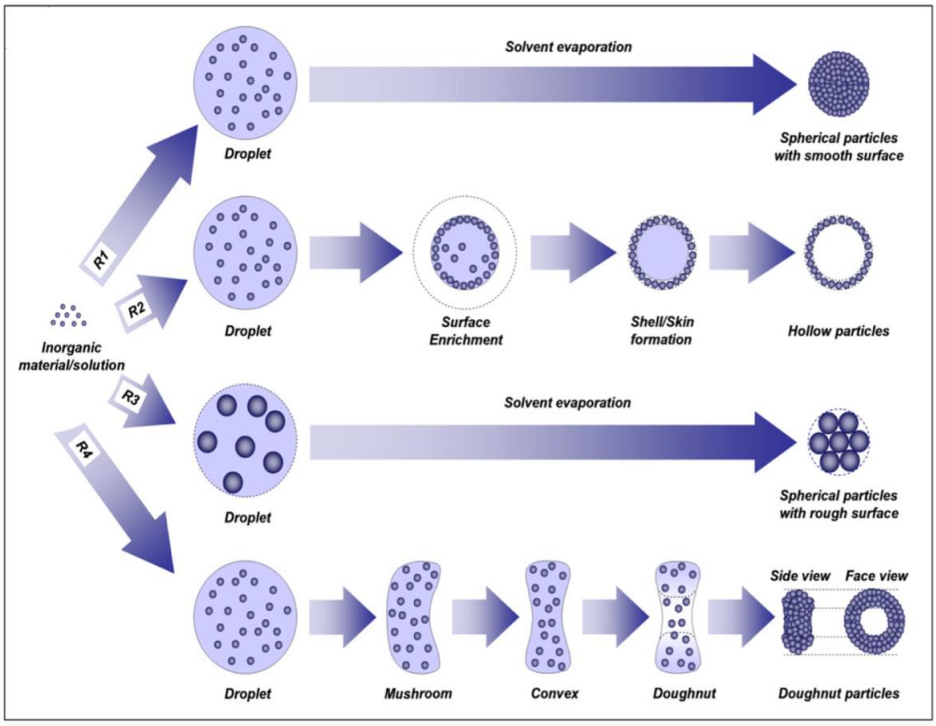

Figure 22. Formation mechanisms of various particle morphologies [70].

The spherical form provides maximum structural stability for the solution. For this reason, spherical form is aimed to be produced. However, different particle morphologies can be obtained by altering several parameters that are related to the mass and the heat transfer of the droplet. Hollow particles can be manufactured by adjusting the parameters for mass and of heat transfer such as characteristic time for solute to reach saturation, heat transfer which is from the surface to the center of droplet and drying residence time as shown in Figure 22-R2 [70].

While the vaporization continues, a portion of the solvent is evaporated before the crust formation. When the amount of evaporated solvent is scaling up, the concentration of solute on the surface of droplet rises. Concurrently, the solute diffuses in the direction of the droplet center and there is a concentration gradient within the droplet as a result. Once the critical supersaturation of the solution is achieved by the concentration of solute on the surface of droplet, the precipitation of solute on the droplet surface stars which is also called as the onset of precipitation. If the solute

concentration of all over the droplet is above the equilibrium saturation of the solution at the droplet temperature at the onset of precipitation, precipitation is volumetric i.e. formation of a fully filled particle occurs.

For other circumstances, hollow particle is formed [68].

By the way, when the increment of initial solute concentration happens, the modification of the solute distribution of concentration within the droplet is observed. The reason of this is that the concentration of solute at a major portion of the droplet is higher than the equilibrium saturation, so the precipitation and growth of solute in a major portion of the droplet take place and a hollow particle has thicker-wall [68].

3.2 Sintering Treatments

After hollow spherical $Ca_3Co_4O_9$ particles were obtained by ultrasonic spray pyrolysis method, heat treatment was applied to powders for removing residual salt from powders. The parameters of heat treatment were 1123 K during 2 hours at first but after SEM studies, breaking down of hollow spherical particles was determined. After the studies for finding out reason of deformed particles, heat treatment parameters was determined as the reason of deformed particles. Then, heat treatment parameters were studied to obtain hollow spherical particles and 1023 K and 30 minutes were selected as heat treatment parameters for obtaining C349 phase without secondary peaks and undeformed particles.

CHAPTER 4

RESULTS AND DISCUSSION

4.1 Structural Characterization of $Ca_3Co_4O_9$

4.1.1 SEM Characterizations of $Ca_3Co_4O_9$

Figure 23 and 24 show that the SEM images of C349 particles without heat treatment which were prepared 1.5 M, 0.15 M and 0.015 M.

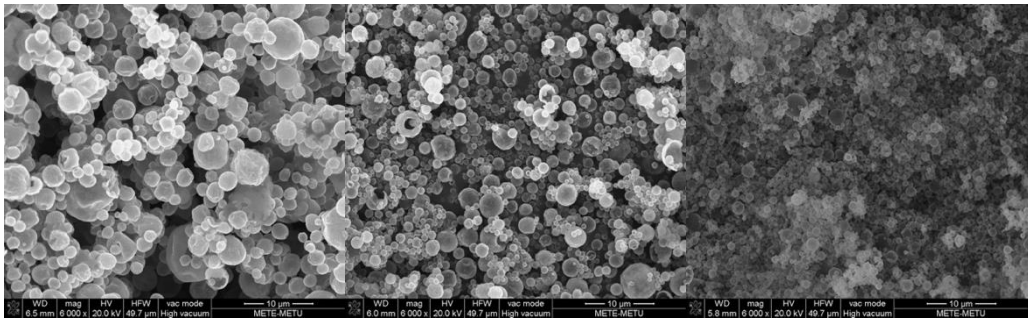

(a) (b) (c)

Figure 23. The SEM images of C349 particles before any treatment (a) 1.5M (b) 0.15M and (c) 0.015M.

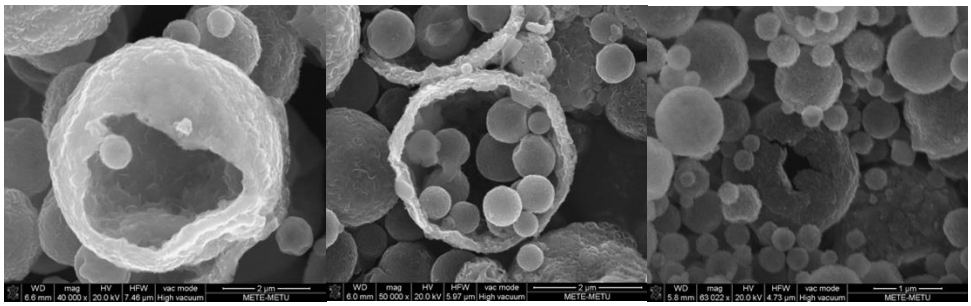

(a) (b) (c)

Figure 24. The SEM images of C349 particles before any treatment (a) 1.5M (b) 0.15M and (c) 0.015M.

According to Figure 23, particle size of 1.5 M, 0.15 M and 0.015 M C349 are about 2.3 μm, 1.5 μm and 500 nm. The particle size decreases as molarity of solution declines because nucleation and growth take place simultaneously [73] and when the amount of precursors is little which means that molarity is less, there is no enough precursors to grow particle.

Determination of Breaking Down of C349 Hollow Spherical Particles

1.5 M, 0.15 M and 0.015 M C349 powders were ground and cold-pressed into pellets of Ø 13 mm and then these pellets were applied heat treatment at 1123 K during 2 hours. When the SEM images of these pellets were observed, breaking down of hollow spherical structures was determined as shown in Figure 25.

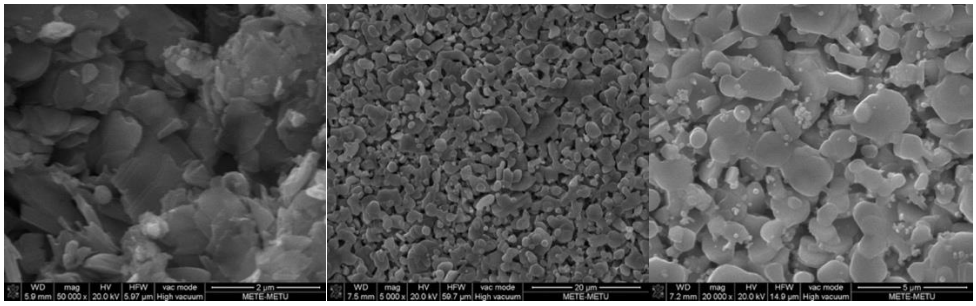

(a) (b) (c)

Figure 25. The SEM images of C349 particles after grinding, cold pressing and heating treatment at 1123 K during 2 hr (a) 1.5M (b) 0.15M and (c) 0.015M.

The Reason of Breaking Down of C349 Hollow Spherical Particles

After that, to figure the reason of breaking down of C349 hollow spherical particles out was the aim. Five samples were prepared which are shown in Table 5. First sample which is shown in Figure 26, the polyvinyl alcohol (PVA) was used as a binder whether or not applied cold press to powder was the reason of breaking down of C349 particles. The C349 powder was ground and then mixed with PVA. After this, it was shaped by mold and put in the furnace at 1123 K during 10 hours. Second sample which is shown in Figure 27, C349 powder was ground and applied heat treatment at 1123 K during 5 hours.

The SEM images of third sample is shown in Figure 28 and this sample was prepared without grinding and has heating treatment at 1123 K during 5 hr. Fourth sample has grinding but no heating treatment and the SEM image of this sample is in Figure 29. The last sample was prepared with PVA after heating treatment at 1123 K during 5 hr and without grinding. The SEM images of this sample is shown in Figure 30. As illustrated in Figure 26, 27, 28, 29 and 30, the shape of the hollow spherical particles became deformed.

Table 3. Samples according to their treatment applications

	PVA	**Grinding**	**Heat Treatment** **(at 1123 K during 5 hr)**
Sample 1	+	+	+
Sample 2		+	+
Sample 3			+
Sample 4		+	
Sample 5	+		+

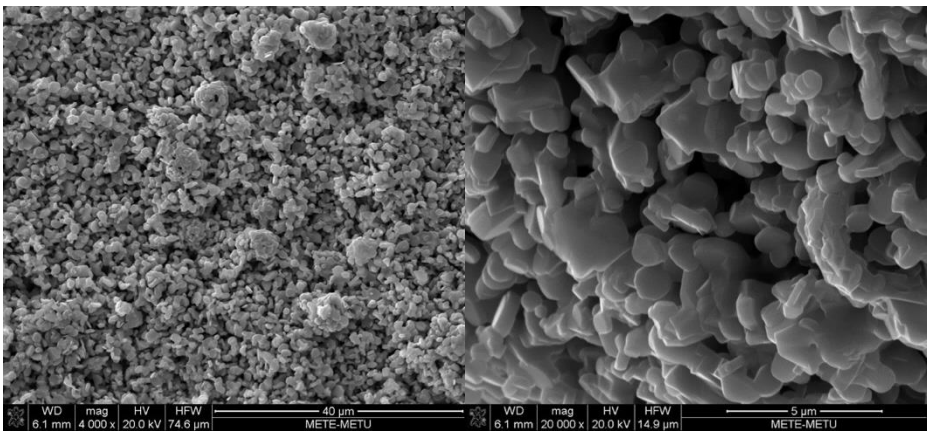

Figure 26. The SEM images of 1.5M C349 particles prepared with PVA after grinding and heating treatment at 1123 K during 10 hr.

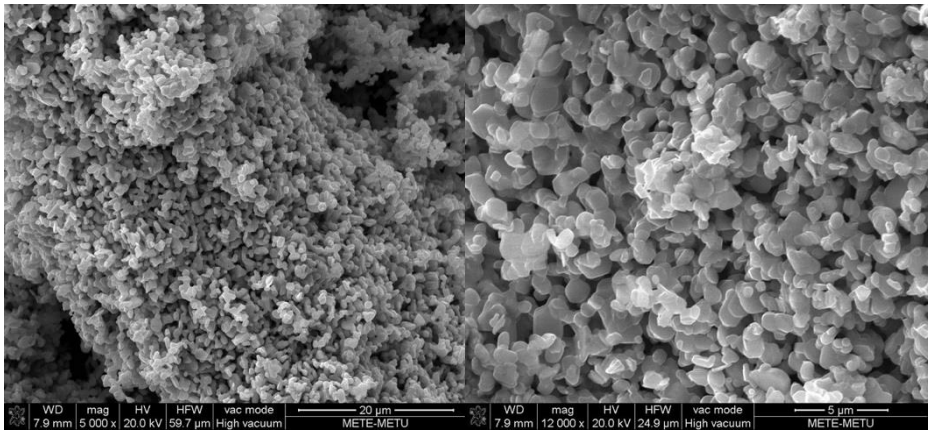

Figure 27. The SEM images of 1.5M C349 particles after grinding and heating treatment 1123 K during 5 hr.

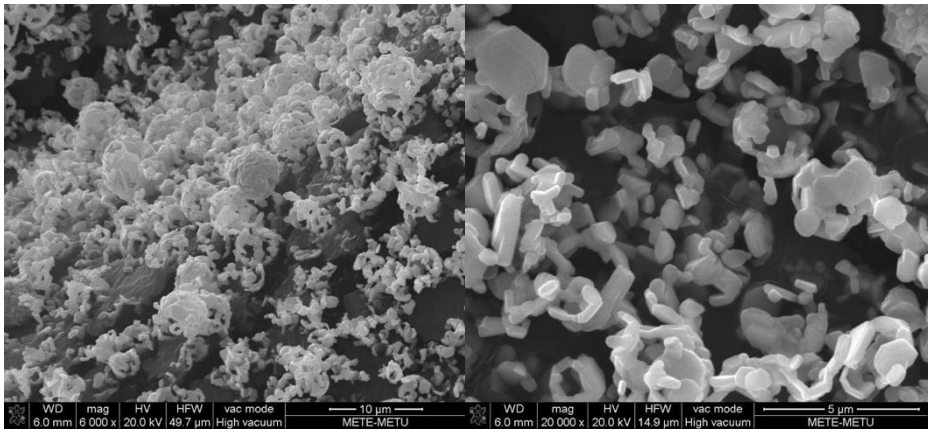

Figure 28. The SEM images of 1.5M C349 particles without grinding and heating treatment 1123 K during 5 hr.

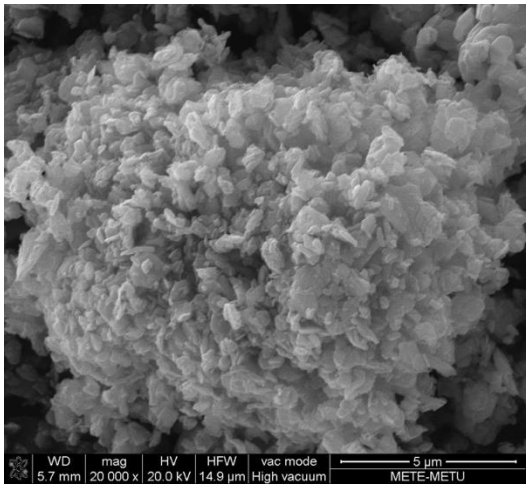

Figure 29. The SEM image of 1.5M C349 particles after grinding and without heat treatment.

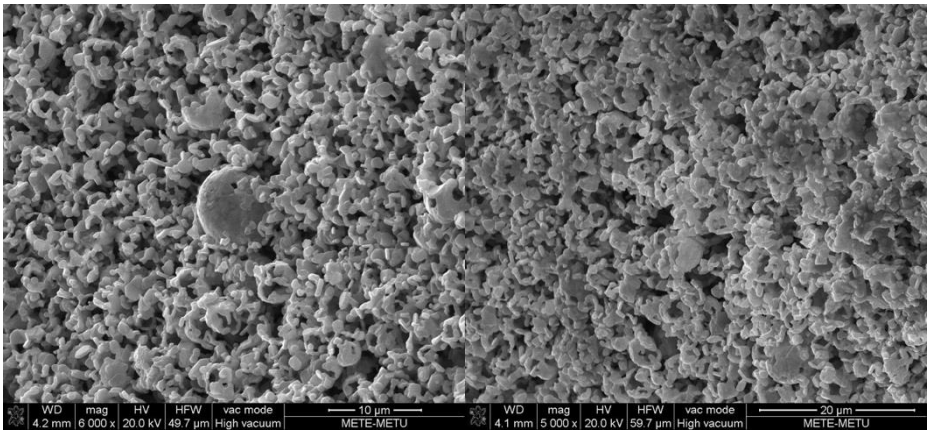

Figure 30. The SEM images of 1.5M C349 particles prepared with PVA after heating treatment 1123 K during 5 hr and without grinding.

Studying on Heating Treatment Parameters

According to these studies, the cause of breaking down of C349 hollow spherical particles was not grinding, cold pressing or using PVA as a binder, so heating treatment was determined the reason of breaking down of C349 microstructures. For this reason, the experiments were done to get optimum parameters which were for temperature and time.

Table 4. Samples according to heating treatment parameters

	Temperature (K)	Time (min)
Sample 1	973	30
Sample 2	973	120
Sample 3	998	30
Sample 4	998	60
Sample 5	998	120
Sample 6	1023	5
Sample 7	1023	15
Sample 8	1023	30
Sample 9	1023	60
Sample 10	1023	120
Sample 11	1048	30
Sample 12	1048	120
Sample 13	1073	5
Sample 14	1123	15

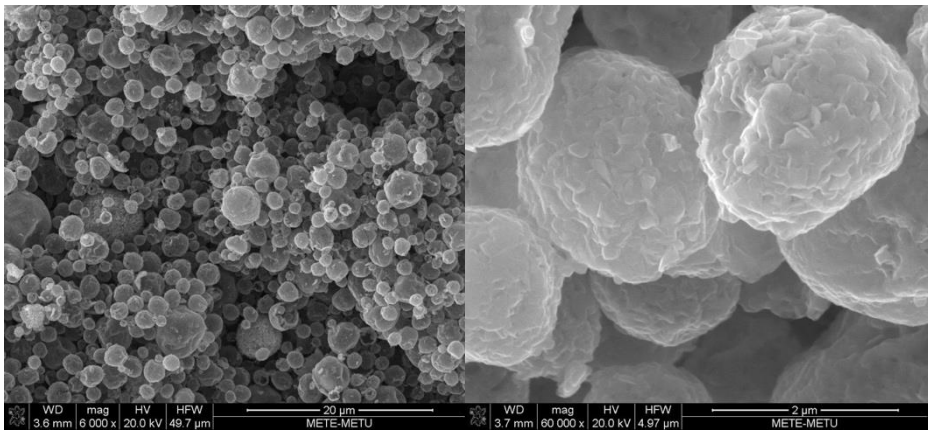

Figure 31. The SEM images of 1.5M C349 particles prepared with PVA after heating treatment 973 K during 30 min.

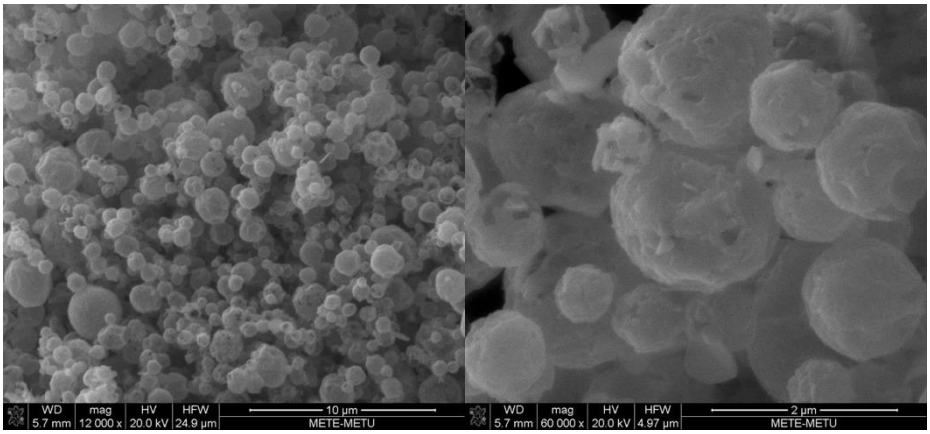

Figure 32. The SEM images of 0.15M C349 particles prepared with PVA after heating treatment 973 K during 2 hr.

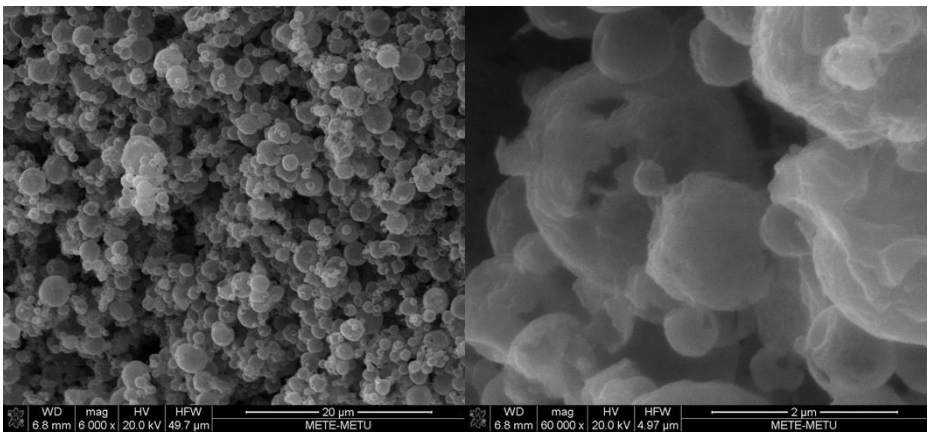

Figure 33. The SEM images of 0.15M C349 particles prepared with PVA after heating treatment 998 K during 30 min.

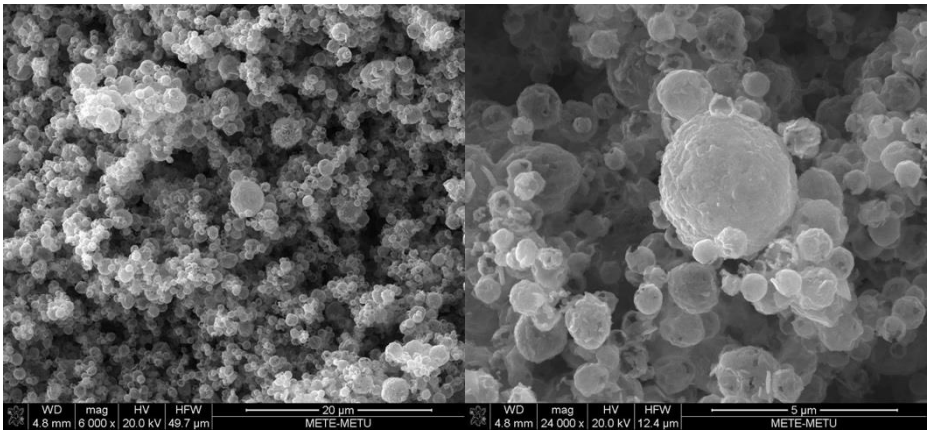

Figure 34. The SEM images of 0.15M C349 particles prepared with PVA after heating treatment 998 K during 60 min.

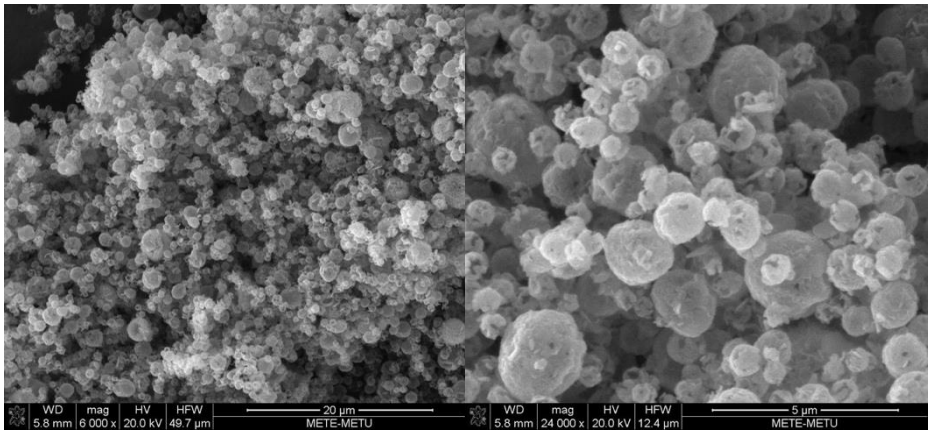

Figure 35. The SEM images of 0.15M C349 particles prepared with PVA after heating treatment 998 K during 2 hr.

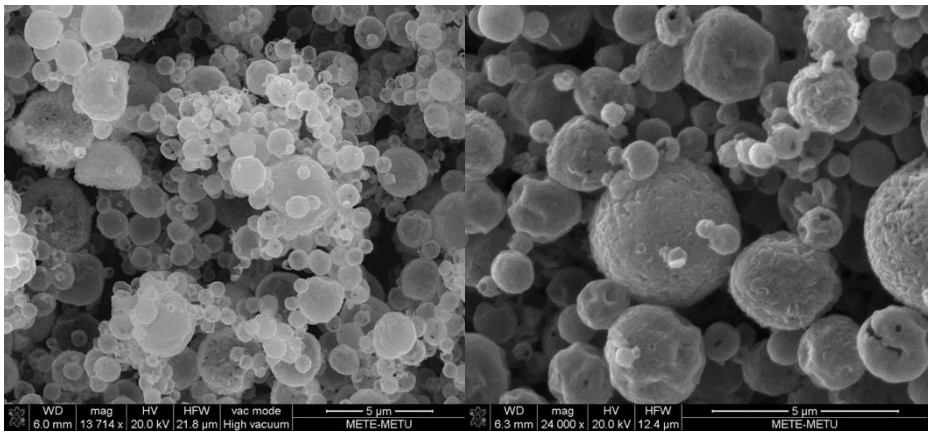

Figure 36. The SEM images of 0.15M C349 particles prepared with PVA after heating treatment 1023 K during 5 min.

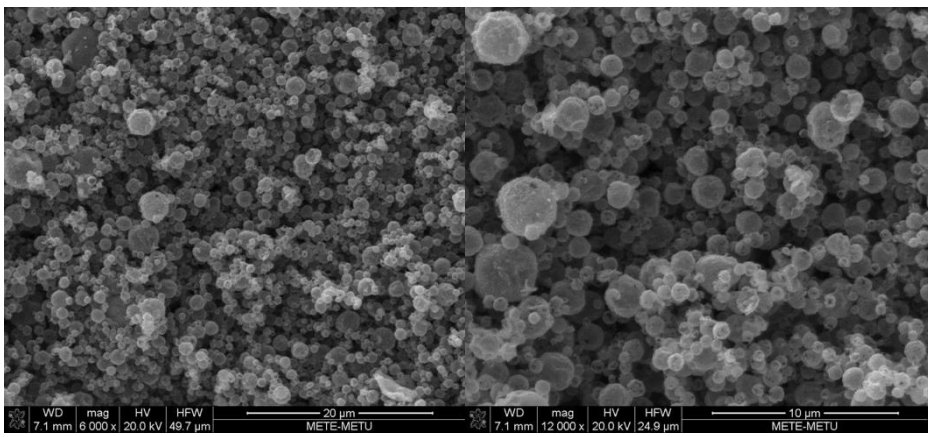

Figure 37. The SEM images of 0.15M C349 particles prepared with PVA after heating treatment 1023 K during 15 min.

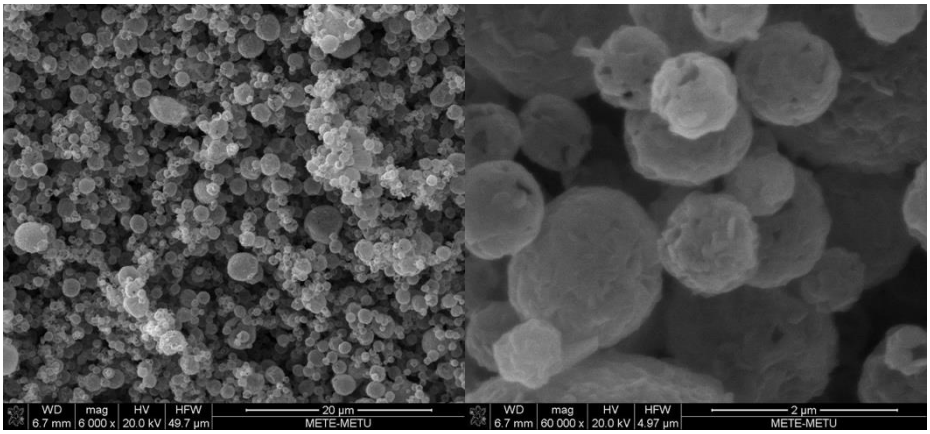

Figure 38. The SEM images of 0.15M C349 particles prepared with PVA after heating treatment 1023 K during 30 min.

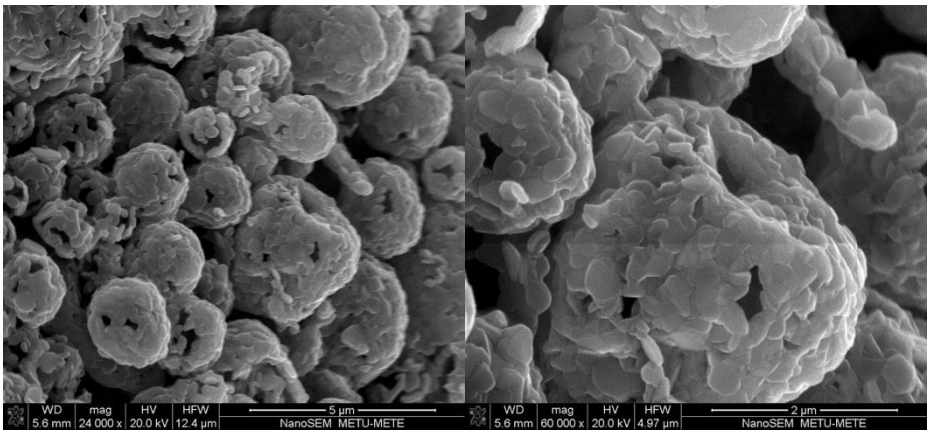

Figure 39. The SEM images of 0.15M C349 particles prepared with PVA after heating treatment 1023 K during 1 hr.

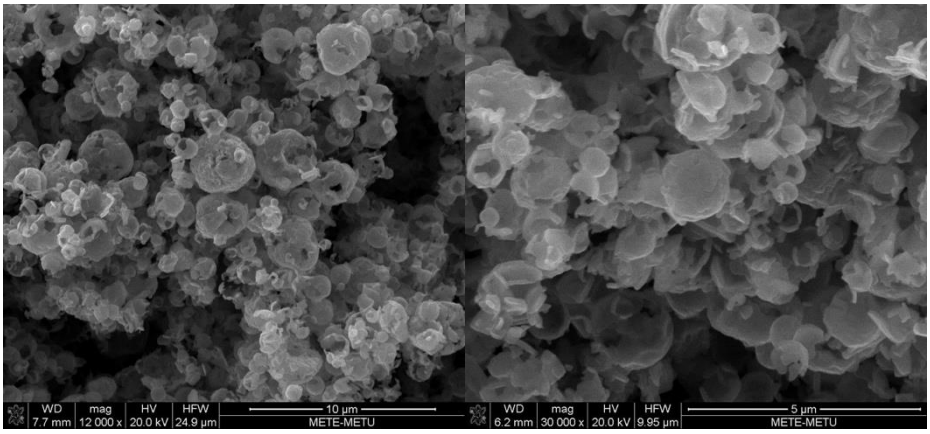

Figure 40. The SEM images of 0.15M C349 particles prepared with PVA after heating treatment 1023 K during 2 hr.

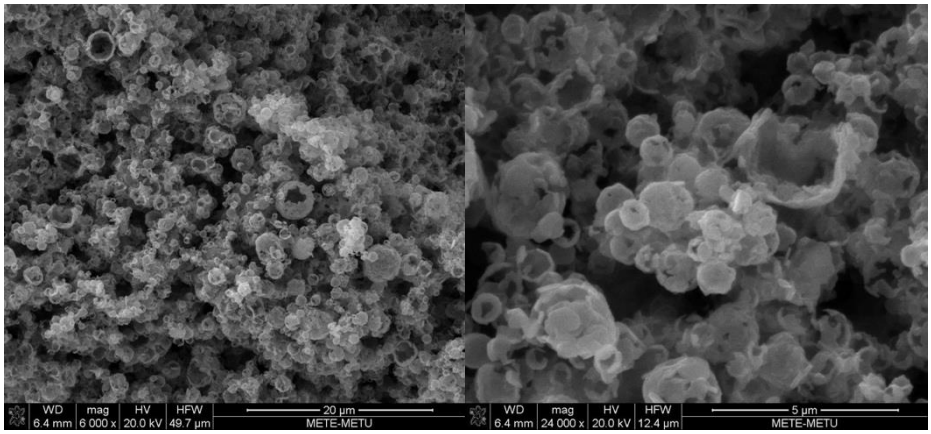

Figure 41. The SEM images of 0.15M C349 particles prepared with PVA after heating treatment 1048 K during 30 min.

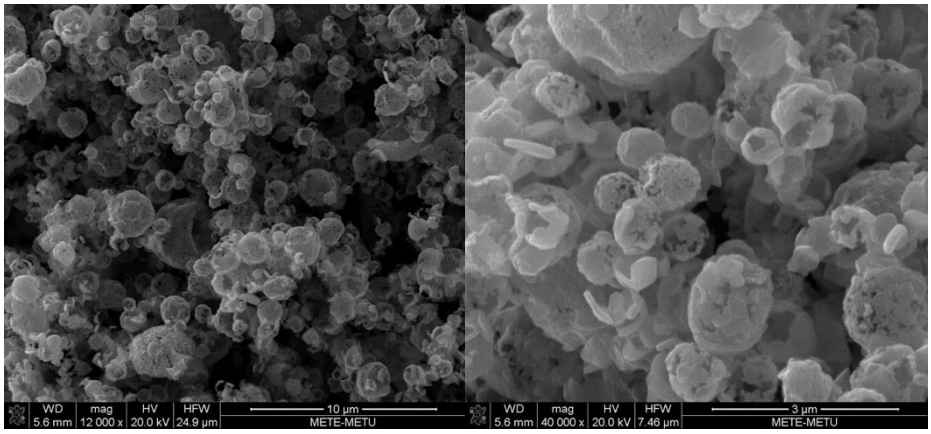

Figure 42. The SEM images of 0.15M C349 particles prepared with PVA after heating treatment 1048 K during 2 hr.

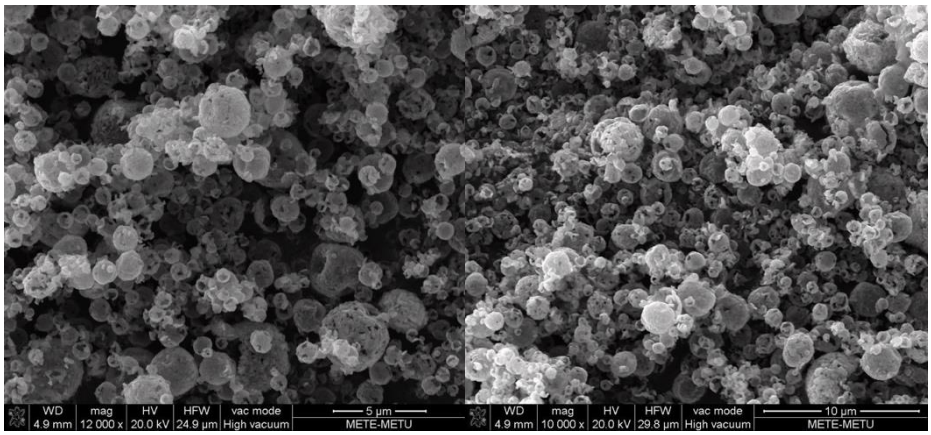

Figure 43. The SEM images of 0.15M C349 particles prepared with PVA after heating treatment 1073 K during 5 min.

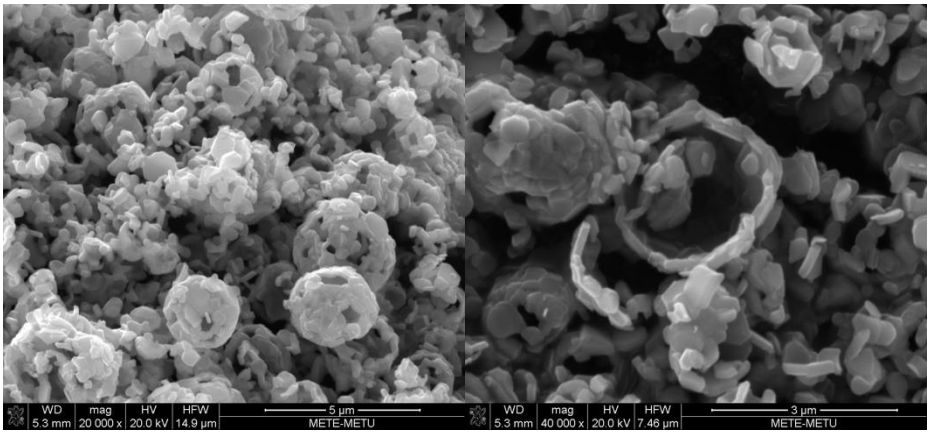

Figure 44. The SEM images of 0.15M C349 particles prepared with PVA after heating treatment 1123 K during 15 min.

The parameters which are 1023 K and 30 minutes are selected for heating treatment because hollow spherical particles form and C349 phase can be obtained without secondary peaks at these parameters which is shown in Figure 38. Moreover, PVA is nonexistence at 1023 K because the boiling point of polyvinyl alcohol is 501 K and PVA does not cause any deformation morphologically according to Figure 45 and 46.

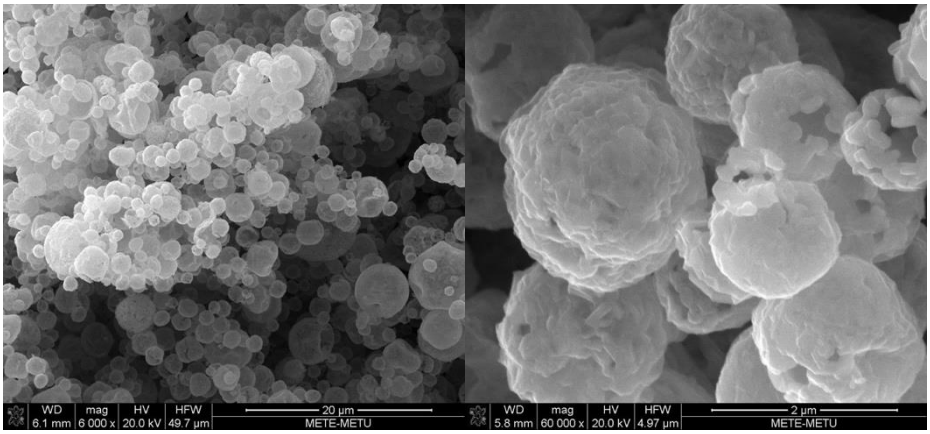

Figure 45. The SEM images of 1.5M C349 particles prepared without PVA after heating treatment 1023 K during 30 min.

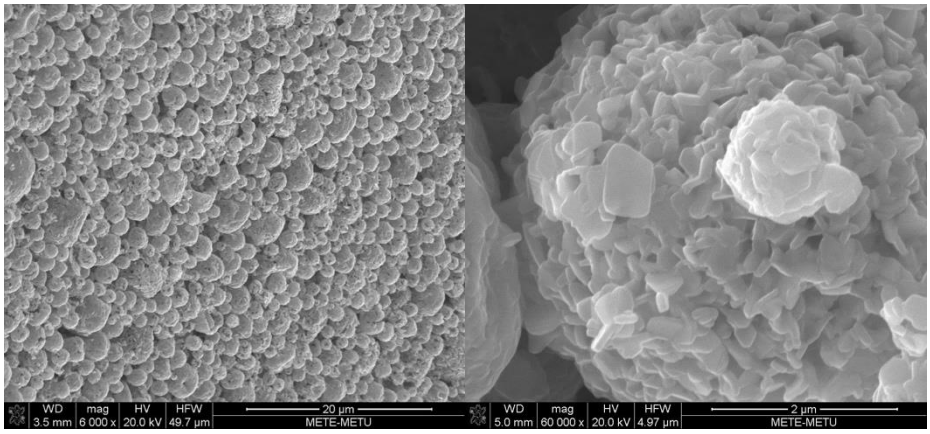

Figure 46. The SEM images of 1.5M C349 particles prepared with PVA after heating treatment 1023 K during 30 min.

4.1.2 Particle Size Analysis

According to SEM images, particle size of 1.5 M, 0.15 M and 0.015 M C349 are about 2.3 μm, 1.5 μm and 500 nm.

According to Figure 47, particles size changes with changing molarity. When the molarity decreases, particle size decreases, too. For 0.015M C349, agglomeration can be observed. The reason of the agglomeration can be explained by the reduction of the size of the spheres, which tend to come together and form large aggregates, seen as a tail in the size distribution diagram given in Figure 47.

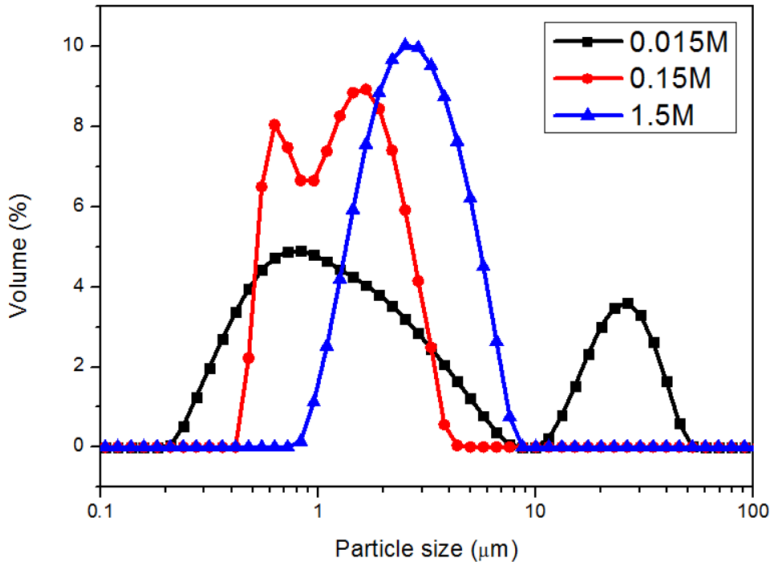

Figure 47. Particle size distribution of particles prepared with 0.015M, 0.15M, 1.5M

Crystallite size analyses were done from X-ray diffraction pattern of 0.015 M, 0.15 M and 1.5 M C349 samples which is shown in Figure 48. Mean crystallite sizes were calculated from Debye-Scherrer formula which uses the line broadening of the peaks for doing analysis of particle size. The results varies from 1.4 to 3.8 nm in the range of 0.015 M to 1.5 M, which are also consistent with SEM image of 1.5 M particles as highlighted in Figure 49. The results of structural analyses of samples are given in Table 5.

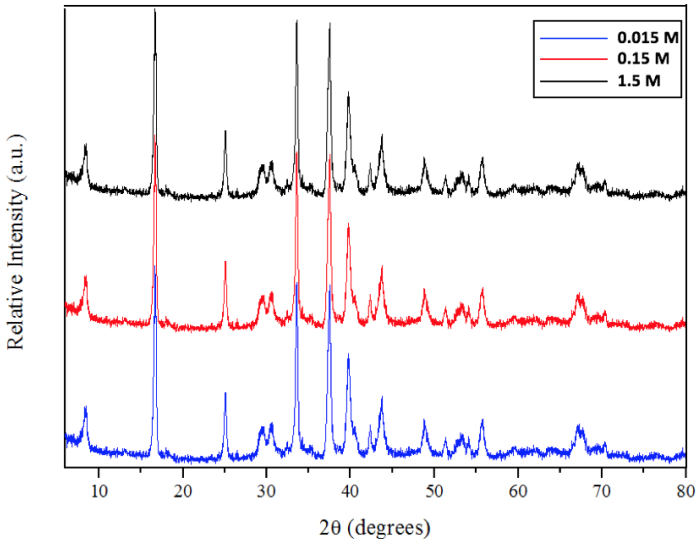

Figure 48. X-ray diffraction pattern of 0.015M, 0.15M and 1.5M C349 sample.

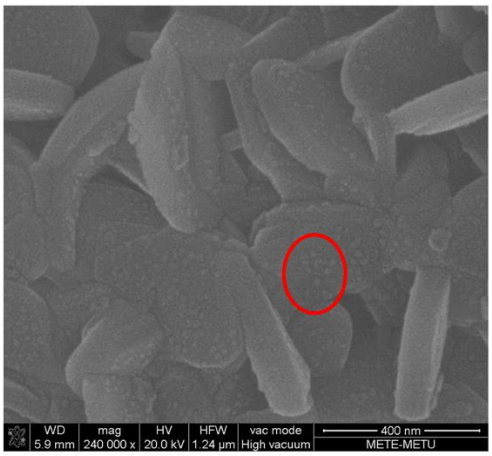

Figure 49. The SEM images of 1.5M C-349 particles prepared with PVA after heating treatment 1023 K during 30 min

Table 5. Structural analyses of samples

	0.015 M	**0.15 M**	**1.5 M**
SEM	500 nm	1.5 µm	2.3 µm
Diffraction	800 nm	1.7 µm	2.5 µm
Crystallite Size Analysis from XRD	1.4 nm	2.1 nm	3.8 nm

4.1.3 XRD Analysis of $Ca_3Co_4O_9$

With respect to Figure 50, $Ca_3Co_4O_9$ phase without secondary peaks can be achieved as expected after heat treatment at 1023 K during 30 min.

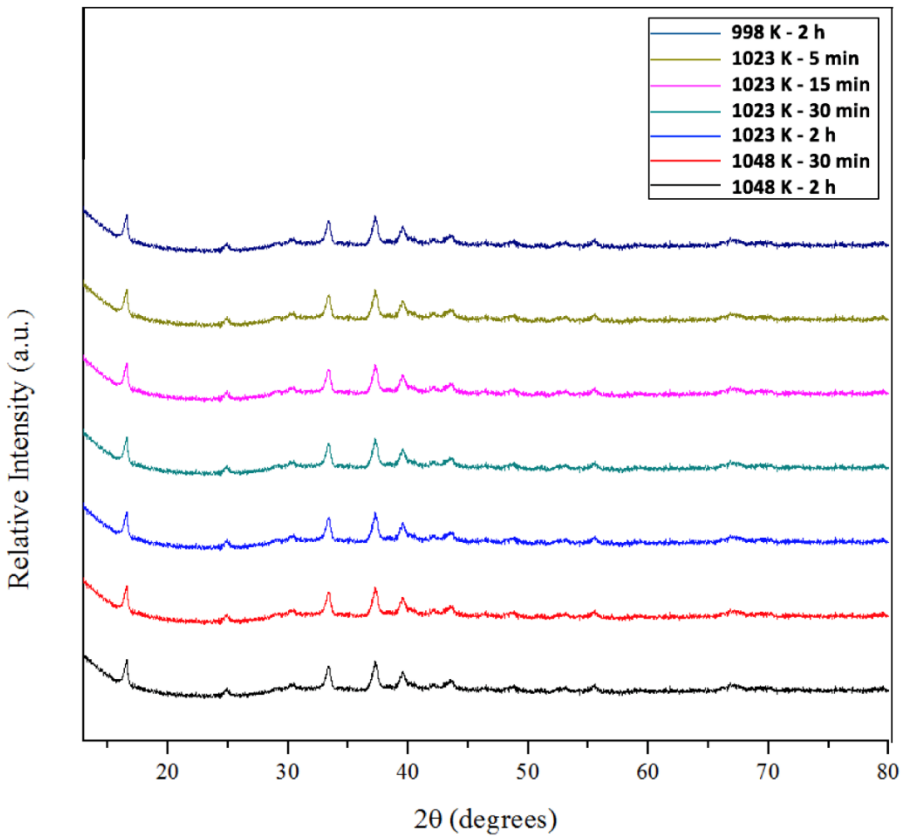

Figure 50. X-ray diffraction pattern of 0.15M C349 sample with heating treatment at different temperatures during different time.

4.1.4 EDS Analysis of $Ca_3Co_4O_9$

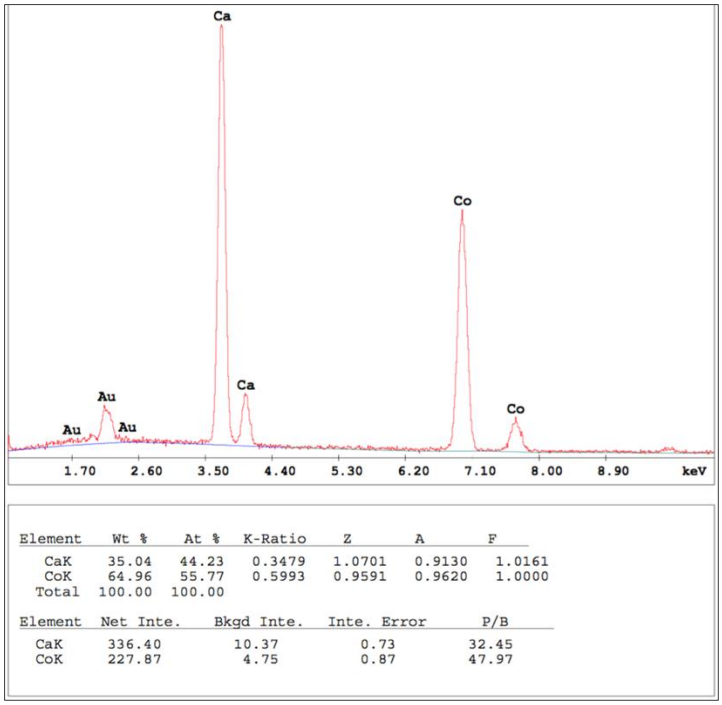

Figure 51. The EDX image of 1.5M C349 particles prepared with PVA after heating treatment 1023 K during 30 min.

With respect to Figure 51, EDS (energy dispersive spectroscopy) result indicates that elemental distribution of the sample. The sample composes of Ca and Co elements as expected.

Table 6. Chemical composition of the sample

Element	Weight%	Atomic%
Ca K	35.04	44.23
Co K	64.96	55.77

4.2 Thermoelectric Properties of Hollow Spherical $Ca_3Co_4O_9$ Particles

The optimal pathway of heat transfer through material is determined according to the thermal conductivities of components of the material.

If the material has pores/bubbles having lower thermal conductivities within a higher thermal conductivity medium, heat moves through the matrix having high conductivity and avoids air bubbles as shown in Figure 52 [74]. A possible increment in ZT was maintained by using structures with microscale porous that leads to a 30% rise in proportion to σ to κ [75]. On the other hand, according to the studies, increasing porosity contributes negatively to electrical conductivity [76].

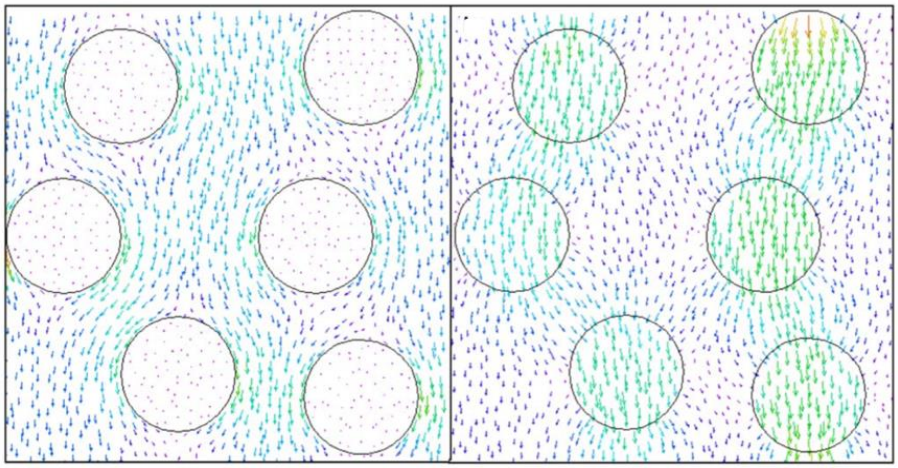

Figure 52. The way of heat flux vectors according to thermal conductivities of the dispersed phase and continuous phase [74].

Maxwell-Eucken equation can be used estimating the porosity effect on thermal conductivity and it is defined as,

$$\kappa = \kappa_0 \frac{1 - P}{1 + \beta P} \qquad (11)$$

where P, κ_0 and β are porosity, the bulk conductivity and the constant number that is determined by the conditions of the pores, respectively. β is taken between 1.0 and 3.0 when the pores are nearly spherical [76]. It means that increasing porosity leads to decreasing thermal conductivity. In this study, thanks to hollow structures of the particles, the particles are filled with air and thanks to pressure-less sintering method, porosity gets very high, so the particles are surrounded by air, too. By means of these, heat flow is obstructed by air having low thermal conductivity.

The thermal conductivities of $Ca_3Co_4O_9$ prepared by a pressure-less sintering/annealing method and air at 300 K are about 1 $W.m^{-1}.K^{-1}$ and 0.026 $W.m^{-1}.K^{-1}$, respectively according to literature [52,77]. Therefore, pores bring about reduction of thermal conductivity dramatically.

According to Raghavan et al., thermal conductivity dramatically decreases with the effect of porosity [78].

Nanostructuring is effective approach for thermoelectric materials to reduce thermal conductivity. According to the many studies, ZT can be enhanced by nanostructuring mainly because of the decrease in thermal conductivity [76].

According to the studies in recent years, enhancing ZT is possible in nanoscale systems through obtaining phonon scattering at interfaces which results in the decrease of κ and quantum confinement and effects of carrier scattering that bring about step-up of the power factor [79].

The aim of much of the recent studies has been enhancing thermoelectric materials based on nanostructuring because of advantages of interfaces. Changing of S, σ and κ is affected by interfaces and interfaces have great effects on nanometarials when nanometarials have interfaces with high density [79].

Thanks to interfaces within a TE material, the thermal conductivity reduces. In addition to that, under certain circumstances, Seebeck coefficient increases because of interfaces. On the other hand, they usually lead to enhance the electrical resistivity [79].

Using for practical applications, TE properties of materials should be further developed. Bulk materials which contain nanoscale constituents can be option for this purpose. In these materials, multiscale effects are produced by the interfaces of nanoscale components. These effects are quantum confinement of electrons that increases the Seebeck coefficient because of DOS which is the large density of states in systems having lower dimension, energy filtering that enhances the power factor because of interface scattering of electrons having low-energy and phonon scattering at interfaces that reduces lattice thermal conductivity [80]. The explanation of the

energy filtering effect on enhancing the Seebeck coefficient is that the electrons having energy higher than the Fermi energy bring about increase in Seebeck coefficient, while the electrons having energy lower than the Fermi energy cause decrease in electrical conductivity [80].

According to the study of Dresselhaus et al. [81], increasing the power factor of material and reducing thermal conductivity of it at the same time only takes place for nanostructured systems. The goals of using nanomaterials into recent researches include to increase ZT via nanomaterials or nanostructures and to improve the density of states near the Fermi energy by quantum confinement effects [82].

These hollow spherical particles have about 2D surface structures and contain nanostructured constituents. Dimensionality has an essential role on the material properties. The limit of ZT around unity is broken by low-dimensional materials which have tremendously high ZT [83].

There are two strategies that are enhancing Seebeck coefficient and controlling Seebeck coefficient and electrical conductivity somewhat severally by using quantum-confinement phenomena and reducing thermal conductivity due to scattering phonons contributing most strongly to the thermal conductivity more effectively than electrons thanks to numerous interfaces to define the effects of low dimensional structures on thermoelectric properties [81].

The quantum confinement concept offers additional degrees of freedom that improves the thermoelectric performance due to the strong correlation between electronic density of states and dimensionality. For instance, decreasing the dimensionality of a 3D sample to 2D quantum wells leads to the new variance of layer thickness that controls material properties [32].

The aim of using low-dimensional structures is obtaining great reduction in the thermal conductivity and suppressing the reduction of electrical conductivity [82].

For low dimensional structures, there are two ideas which are dominant. One of them is that nanoscale constituents brings about quantum confinement effects which increase the power factor. Other one is that there are lots of internal interfaces which

are found in nanostructures, so the thermal conductivity decreases more than the electrical conductivity because of differences in scattering lengths of them [81]. When the phonons scatter more strongly than electrons at interfaces, structures having interfaces are favourable for thermoelectric materials due to enhancement in *ZT* [79]. For scattering of phonons and electrons that have long mean-free-path, interfaces are effective. However, when the spacing between interfaces are longer than the mean-free-paths, interfaces have small effect [79].

For quantum well structure at comparatively high temperatures, dominant scattering mechanism blocking heat flow is three-phonon interaction. The processes such as impurity scattering, the three-phonon umklapp scattering process and boundary scattering which do not conserve the momentum lead to the decrease in lattice thermal conductivity [84].

The rate of umklapp scattering in a quantum well increases due to phonon dispersion modification which is based on spatial confinement of the phonon modes [84].

When the size of system reduces to nanometer length scales, the marked differences is observed in the density of electronic states. When the length scale decreases adequately to bring about quantum-confinement effects, Seebeck coefficient, electrical conductivity and thermal conductivity can change independently [81].

According to a theoretical study, significant enhancement in electronic properties can be achieved by using 2, 1, or 0 dimensional structures and comparing them with what was thought to be attainable in bulk materials. Also, thanks to using nanostructures, significant decrease in lattice thermal conductivity can be obtained [2]. By this study, it is seen that the achievement was far more successful.

Electronic density of states changes considerably due to quantum confinement effect, while the dimension of materials reduces and approximates nanometer length scales. To enhance thermoelectric performance of materials, Seebeck coefficient is improved because of increased electronic DOS. Equation 10 is Mott expression which shows that S is based on the energy derivative of energy-dependent electrical conductivity which is defined as $\sigma = n(E)q\mu(E)$, where $n(E)$ is the carrier density at the energy level

E considered, q is the carrier charge and $\mu(E)$ is the mobility. $n(E)$ is defined as $n(E)=g(E)f(E)$, where $g(E)$ is the DOS per unit volume and per unit energy and $f(E)$ is the Fermi function [83]. Also, Seebeck coefficient depends on the energy derivative of the electronic density of states $N(E)$ and the scattering (relaxation) time τ according to the Mott expression. The electronic group velocity is v [79].

$$S = \frac{\pi^2 k_B}{3q} k_B T \left\{ \frac{d[\ln(\sigma(E))]}{dE} \right\}_{E=E_F}$$

$$= \frac{\pi^2 k_B}{3q} k_B T \left\{ \frac{1dn(E)}{n\,dE} + \frac{1d\mu(E)}{\mu\,dE} \right\}_{E=E_F} \qquad (12)$$

$$= \frac{\pi^2 k_B^2 T}{3q} \left(\frac{d \ln N(E)}{dE} + \frac{d \ln \tau(E) v(E)^2}{dE} \right)_{E=E_F}$$

Two mechanisms that are an enhanced energy-dependence of $\mu(E)$ and an enhanced energy-dependence of $n(E)$ can enhance S with reference to the Mott relation. For instance, energy-dependence of $n(E)$ can be increased by a local enhance in $g(E)$. For materials with lower dimension, Seebeck coefficient is mainly improved by second mechanism [83]. Sharp vicissitudes in the electronic DOS which bring about the increase in S and ZT are created by quantum size effects [79]. As a consequence of this, enhanced power factor is obtained.

For p-type conduction which have holes, the Seebeck coefficient is positive and for n-type conduction which have electrons, the Seebeck coefficient is negative [3].

The quantum confinement effect is influence on not only carriers with increment in power factor but also phonons which causes strong modification on phonon group velocity. A significant enhancement in the phonon relaxation rates which causes decreased the thermal conductivity is attained by strong modification of phonon group velocities because of the quantum confinement in quantum well. Also, the phonon scattering at interfaces becomes substantial due to reducing dimension of materials. Hence, ZT can be further improved due to diminution of lattice thermal conductivity of materials [83].

For solid solutions, phonons having high-frequency and short-wavelength are scattered exceedingly due to point imperfections, so heat is conducted mainly by the phonons having a long free path, low-frequency, long-wavelength and being especially responsive to scatter by grain boundaries [31]. Nanostructuring causes to suppress phonon scattering which have long-wavelength at grain boundaries, so the phonon thermal conductivity reduces.

As regards theoretical predictions, phonons have selective scattering stronger than charge carriers and it causes to improve thermoelectric properties [76]. The thermal conductivity decreases in spite of suppressing the reduction of electrical conductivity thanks to using low-dimensional structures. For instance, the electrical conductivity enhances in 2D structures, while the thermal conductivity reduces for nanoscale SnS_2 [82].

Reducing particle dimensions to the order of several nanometers causes remarkable deviation from the physical and chemical properties of such bulk materials. However, the materials suffer from some difficulties related to handling, thermal stability and surface stability of them, saving shape and assembly in devices because of the small sizes they have [69]. Therefore, the aim is getting larger particles which have properties of nanoscale material.

According to Li et al., when the temperature rises, the total thermal conductivity is reduced by phonon scattering due to Umklapp for compounds which are crystalline [36].

4.2.1 Seebeck Coefficient Measurements

Seebeck coefficients of materials were measured by a homemade setup which consists of a heating unit and two commercial K-type thermocouples.

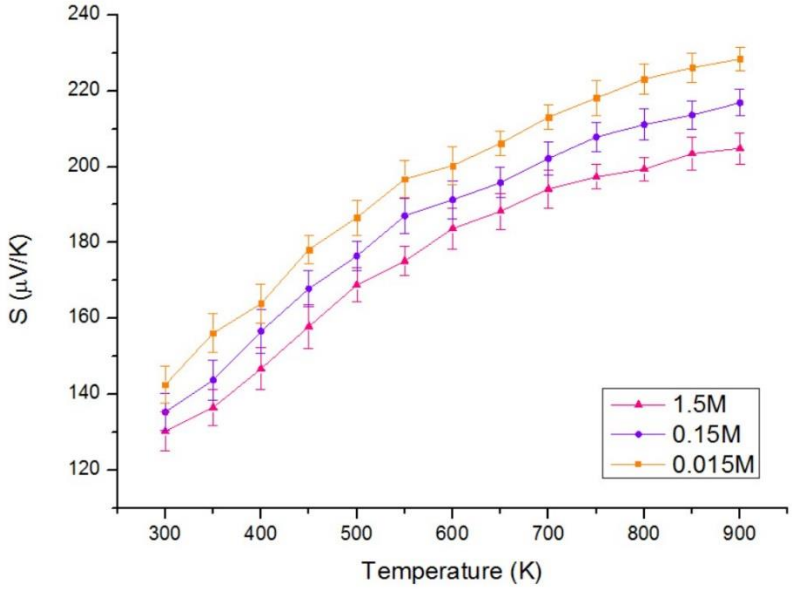

Figure 53. Temperature dependence of Seebeck coefficient of 1.5M, 0.15M and 0.015M C349.

There are two strategies that are enhancing Seebeck coefficient and controlling Seebeck coefficient and electrical conductivity somewhat severally by using quantum-confinement phenomena and reducing thermal conductivity due to scattering phonons contributing most strongly to the thermal conductivity more effectively than electrons thanks to numerous interfaces to define the effects of low dimensional structures on thermoelectric properties [81].

The surface having nanoscale constituents and about 2D provides quantum confinement effect which brings about increase in Seebeck coefficient due to the large density of states in systems having lower dimension and energy filtering which increases the power factor due to interface scattering of electrons having low-energy. Moreover, porous structure provides enhancing Seebeck coefficient when compared to the Seebeck coefficient of dense samples [85]. Therefore, thanks to this structure of $Ca_3Co_4O_9$ particles, high Seebeck coefficient can be achieved relatively.

The temperature dependence of Seebeck coefficient for three samples having different molarity is shown in Fig. 53. As can be seen in this figure, the Seebeck coefficients of the samples increase with rising temperature which means that the dominant carriers

are holes because for p-type conduction which have holes, the Seebeck coefficient is positive and for n-type conduction which have electrons, the Seebeck coefficient is negative [3].

As shown in Fig. 53, the decrease of molarity has an effect on Seebeck coefficient positively because when the molarity decreases, particle size decreases, too. Therefore, nanoscale constituents of surface of hollow spherical particles become smaller and surface of particles approaches being 2D much more than others. Also, higher porosity is obtained through samples having small grain size [76].

4.2.2 Resistivity Measurements

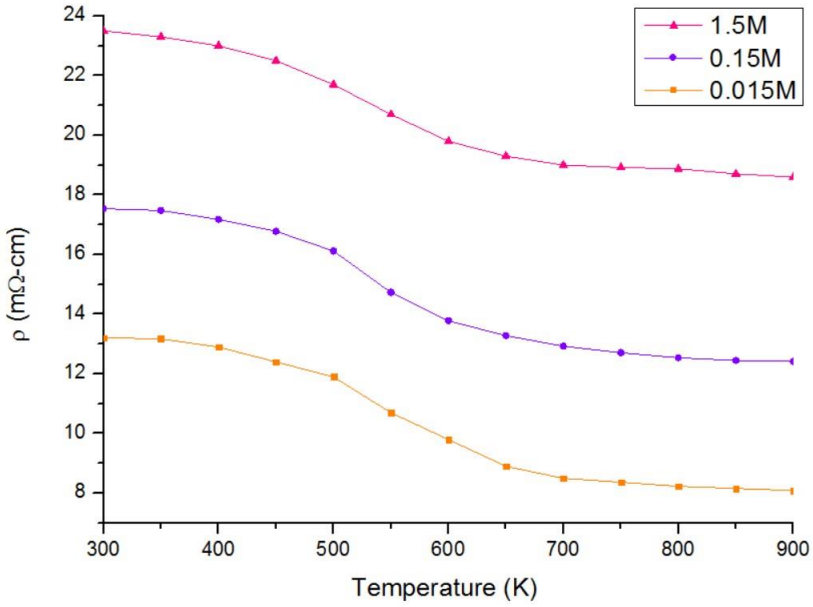

Figure 54. Temperature dependence of electrical resistivity of 1.5M, 0.15M and 0.015M C349.

As shown in Fig. 54, when the temperature increases, electrical resistivity decreases for all samples which indicates a semiconducting-like behavior. Thanks to interfaces within a TE material, the thermal conductivity reduces. On the other hand, they can lead to enhance the electrical resistivity [79]. However it does not effect as much as thermal conductivity due to differences in scattering lengths of them. Also, increasing

porosity causes decreasing electrical conductivity [76]. However, the aim of using low-dimensional structures is obtaining not only great reduction in the thermal conductivity but also suppressing the reduction of electrical conductivity [82]. As regards theoretical predictions, phonons have selective scattering stronger than charge carriers and it causes to improve thermoelectric properties [76]. Electrical resistivity decreases with decrease in molarity as shown in Fig. 54. However, porosity and density of interface increase with reducing molarity and these affect electrical conductivity negatively. Therefore, the reason of these results can be the surfaces of hollow spherical particles which approach being 2D when the molarity decreases. It means that the dominant effect on electrical conductivity is low-dimensional structure.

For instance, the electrical conductivity enhances in 2D structures, while the thermal conductivity reduces for nanoscale SnS_2 [82].

4.2.3 Power Factor Calculations

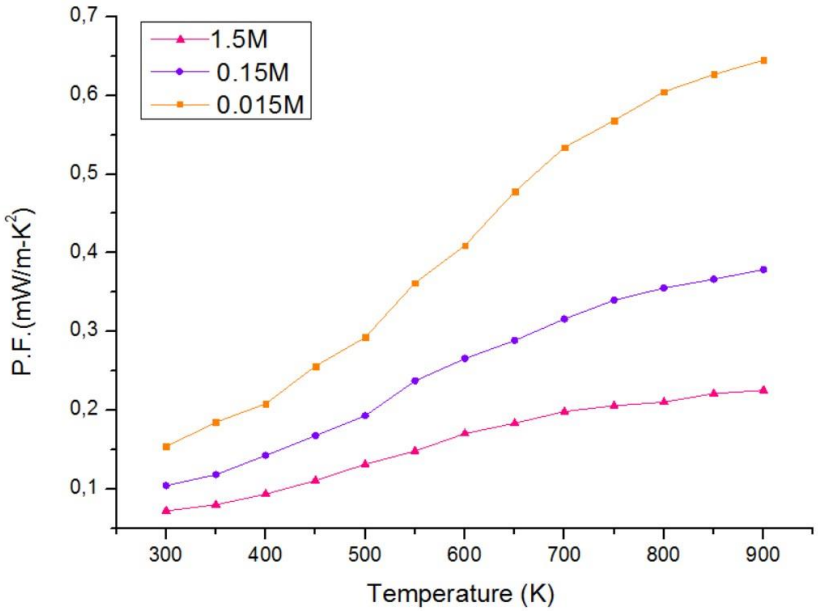

Figure 55. Temperature dependence of power factor of 1.5M, 0.15M and 0.015M C349.

The temperature dependence of power factor for three samples having different molarity is shown in Fig. 55. As can be seen, power factor increases with increasing

temperature and reducing molarity of initial solution because power factor depends on Seebeck coefficient and electrical conductivity, $PF = \sigma * S^2$. Furthermore, thermal conductivity reduces for obtaining high ZT. For this, effect of porosity and increased density of interface can be used. Changing of S, σ and κ is affected by interfaces and interfaces have great effects on nanometarials when nanometarials have interfaces with high density [79]. Nanostructuring is effective approach for thermoelectric materials to reduce thermal conductivity. According to the many studies, ZT can be enhanced by nanostructuring mainly because of the decrease in thermal conductivity [76]. For quantum well structure at comparatively high temperatures, dominant scattering mechanism blocking heat flow is three-phonon interaction. The processes such as impurity scattering, the three-phonon umklapp scattering process and boundary scattering which do not conserve the momentum lead to the decrease in lattice thermal conductivity [84].

The rate of umklapp scattering in a quantum well increases due to phonon dispersion modification which is based on spatial confinement of the phonon modes [84]. According to Raghavan et al., thermal conductivity dramatically decreases with the effect of porosity [78].

Table 7. Thermoelectrics measurements of samples at 900 K

	0.015 M	**0.15 M**	**1.5 M**
Seebeck Coefficient (μV/K)	228.39	216.87	204.81
Electrical Resistivity (mΩ-cm)	8.09	12.42	18.6
Power Factor (mW/m-K^2)	0.64	0.38	0.23

Seebeck coefficients of the samples having 2.3 μm, 1.5 μm and 500 nm diameter at 900 K are 204.8 μV/K, 216.9 μV/K and 228.4 μV/K, respectively. Electrical resistivities of the samples having 2.3 μm, 1.5 μm and 500 nm diameter at 900 K are measured as 18.6 mΩ.cm, 12.4 mΩ.cm and 8.1 mΩ.cm, respectively. Power factors of the samples having 2.3 μm, 1.5 μm and 500 nm diameter at 900 K are 0.23 mW/mK^2, 0.38 mW/mK^2 and 0.64 mW/mK^2, respectively. Table 7 is shown the thermoelectrics measurements of samples at 900 K. It was shown that, by reducing the particle and nanocrystallite size to submicron range, Seebeck coefficient was successfully increased by our air composite approach employed in this work.

CHAPTER 5

CONCLUSION AND SUGGESTIONS

This study draw the attention to the effects of terms porosity, low-dimensional structure and nanoparticle in the bulk materials in order to influence and compare them for the thermoelectric properties of materials. The aim of this study is achieving high ZT value by hollow spherical $Ca_3Co_4O_9$ and air composite materials.

$Ca_3Co_4O_9$ is selected because this material is oxidation resistant, nontoxic, chemically and thermally stable in air, light, environment friendly, having low cost, humidity resistant at high temperatures, and abundant. Also, $Ca_3Co_4O_9$ is favored due to its natural layered structure composing of conduction and insulation layers alternately which provide electronic transport and phonon scattering layers separately. Therefore, natural superlattice structure of $Ca_3Co_4O_9$ brings about high thermopower and low electrical resistivity at the same time.

The selected method is ultrasonic spray pyrolysis method. Many parameters have an effect on forming hollow spherical structure such as frequency of ultrasonic generator, the concentration of initial solution, the temperature of reactor and the flow rate of the carrier gas which are influence on the end product morphology, dispersity, structure and the phase composition. Nanostructural hollow spherical $Ca_3Co_4O_9$ particles were obtained by USP technique because these parameters can be controlled easily thanks to this technique. High evaporation rate and high mass transfer are required for getting hollow spherical structure.

Three varied solutions that were prepared by deionized water, dimethylformamide and methanol were taken. These solvents was chosen according to their capability of making aerosol. According to the capability of making $Ca_3Co_4O_9$ phase without secondary peaks, being nontoxic and eco-friendly, deionized water was determined as solvent. Then, different temperatures for tube furnace were tested for determine the operating temperature to get hollow spherical C349 particles with totally C349 phase.

1173 K was chosen for tube furnace operating temperature. After formed hollow spherical structure, particles were ground, pelletized via cold pressing and subjected to heat treatment at 1123 K during 2 hours due to removing residual salt from the structure. $Ca_3Co_4O_9$ phase was obtained with these but hollow spherical structure could not be obtained, particles broke down, so studies were done to determine the reason of breaking down of $Ca_3Co_4O_9$ particles. Five samples were prepared with respect to underwent grinding, heat treatment or being pellet via binder which was PVA instead of cold pressing. According to SEM images of these five samples, the reason of deformed particles is the parameters of heat treatment, so 14 samples were prepared at different temperatures with different process time. After these experiments, 1023 K and 30 minutes are chosen as the parameters of heat treatment due to providing unbroken $Ca_3Co_4O_9$ particles with fully $Ca_3Co_4O_9$ phase without secondary peaks.

This structure comprise of hollow spherical $Ca_3Co_4O_9$ particles and many porosities dispersing in the matrix. This means that lots of air having very low thermal conductivity is trapped in the structure, so thermal conductivity of the materials can be decreased. Obtaining high porosity structure was achieved by using pressure-less sintering method. Furthermore, the surfaces of hollow spherical particles comprising of nanoscale constituents are about 2D, so this leads to quantum confinement effect and energy filtering which increase the power factor and phonon scattering at interfaces which decreases lattice thermal conductivity. Therefore, thanks to the increase in power factor and decrease in thermal conductivity, achieving high ZT is expected. Seebeck coefficients of the samples having 2.3 μm, 1.5 μm and 500 nm diameter at 900 K are 204.8 μV/K, 216.9 μV/K and 228.4 μV/K, respectively. Electrical resistivities of the samples having 2.3 μm, 1.5 μm and 500 nm diameter at 900 K are measured as 18.6 mΩ.cm, 12.4 mΩ.cm and 8.1 mΩ.cm, respectively. Power factors of the samples having 2.3 μm, 1.5 μm and 500 nm diameter at 900 K are 0.23 mW/mK^2, 0.38 mW/mK^2 and 0.64 mW/mK^2, respectively. It was shown that, by reducing the particle and nanocrystallite size to submicron range, Seebeck coefficient was successfully increased by our air composite approach employed in this work.

REFERENCES

1. Bell, L. E. Cooling, heating, generating Power, and recovering wast heat with thermoelectric systems. *Science (80-.).* **321,** 1457 (2008).
2. Minnich, A. J., Dresselhaus, M. S., Ren, Z. F. & Chen, G. Bulk nanostructured thermoelectric materials: current research and future prospects. *Energy Environ. Sci.* **2,** 466 (2009).
3. He, J. & Tritt, T. M. Advances in thermoelectric materials research: Looking back and moving forward. *Science (80-.).* **357,** (2017).
4. Yang, J. *et al.* On the tuning of electrical and thermal transport in thermoelectrics: an integrated theory–experiment perspective. *npj Comput. Mater.* **2,** 15015 (2016).
5. Pei, Y.-L. *et al.* High thermoelectric performance in n-type BiAgSeS due to intrinsically low thermal conductivity. *Energy Environ. Sci.* **6,** 1750 (2013).
6. Dughaish, Z. H. Lead telluride as a thermoelectric material for thermoelectric power generation. *Phys. B Condens. Matter* **322,** 205–223 (2002).
7. Hamid Elsheikh, M. *et al.* A review on thermoelectric renewable energy: Principle parameters that affect their performance. *Renew. Sustain. Energy Rev.* **30,** 337–355 (2014).
8. Sun, P. *et al.* Large Seebeck effect by charge-mobility engineering. *Nat. Commun.* **6,** 1–5 (2015).
9. Zhu, P. W. *et al.* A new method of synthesis for thermoelectric materials: HPHT. *Solid State Commun.* **123,** 43–47 (2002).
10. Han, C., Li, Z. & Dou, S. Recent progress in thermoelectric materials. *Chinese Sci. Bull.* **59,** 2073–2091 (2014).
11. Liu, Y. *et al.* Enhanced thermoelectric performance of BiCuSeO composites with nanoinclusion of copper selenides. *J. Alloys Compd.* **662,** 320–324 (2016).
12. Zhao, L.-D. *et al.* BiCuSeO oxyselenides: new promising thermoelectric materials. *Energy Environ. Sci.* **7,** 2900–2924 (2014).

13. He, Z. *et al.* Effect of ceramic dispersion on thermoelectric properties of nano-ZrO 2CoSb3 composites. *J. Appl. Phys.* **101,** (2007).
14. Pele, V., Barreteau, C., Berardan, D., Zhao, L. & Dragoe, N. Direct synthesis of BiCuChO-type oxychalcogenides by mechanical alloying. *J. Solid State Chem.* **203,** 187–191 (2013).
15. Du, Y. *et al.* Thermoelectric fabrics: Toward power generating clothing. *Sci. Rep.* **5,** 1–6 (2015).
16. Wu, J. *et al.* Polypyrrole nanotube film for flexible thermoelectric application. *Synth. Met.* **196,** 173–177 (2014).
17. Tritt, T. M. & Subramanian, M. a. Thermoelectric Materials, Phenomena, and Applications : A Bird' s Eye View. *MRS Bull.* **31,** 188–198 (2006).
18. DiSalvo, F. Thermoelectric cooling and power generation. *Science* **285,** 703–6 (1999).
19. He, J., Liu, Y. & Funahashi, R. Oxide thermoelectrics: The challenges, progress, and outlook. *J. Mater. Res.* **26,** 1762–1772 (2011).
20. Zebarjadi, M., Esfarjani, K., Dresselhaus, M. S., Ren, Z. F. & Chen, G. Perspectives on thermoelectrics: from fundamentals to device applications. *Energy Environ. Sci.* **5,** 5147–5162 (2012).
21. Rowe, D. M. Modern Thermoelectrics. 166 (1983).
22. Rowe, E. D. M., Ph, D., Sc, D. & Group, F. *HANDBOOK*. (2006).
23. Zlatiâc, V. & Hewson, A. Properties and applications of thermoelectric materials. (2009).
24. Hsu, K. F. Bulk Thermoelectric Materials with High Figure of Merit. **818,** 2000–2004 (2010).
25. Poudel, B. *et al.* High-Thermoelectric Performance of Nanostructured Bismuth Antimony Telluride Bulk Allys. *Sci.* **320,** 634–638 (2008).
26. Heremans, J. P., Thrush, C. M. & Morelli, D. T. Thermopower enhancement in lead telluride nanostructures. *Phys. Rev. B - Condens. Matter Mater. Phys.* **70,** (2004).
27. Wang, Y., Sui, Y., Wang, X., Su, W. & Liu, X. Enhanced high temperature thermoelectric characteristics of transition metals doped Ca3 Co4 O9+δ by cold high-pressure fabrication. *J. Appl. Phys.* **107,** 0–9 (2010).

28. Wan, C. *et al.* Development of novel thermoelectric materials by reduction of lattice thermal conductivity. *Sci. Technol. Adv. Mater.* **11,** (2010).
29. Heremans, J. P. *et al.* Enhancement of Thermoelectric of the Electronic Density of States. *Science (80-.).* **321,** 1457–1461 (2008).
30. Harman, T. C., Taylor, P. J., Walsh, M. P. & La Forge, B. E. Quantum dot superlattice thermoelectric materials and devices. *Science (80-.).* **297,** 2229–2232 (2002).
31. Toprak, M. S. *et al.* The impact of nanostructuring on the thermal conductivity of thermoelectric CoSb3. *Adv. Funct. Mater.* **14,** 1189–1196 (2004).
32. Zhang, X. & Pei, Y. Manipulation of charge transport in thermoelectrics. *npj Quantum Mater.* **2,** 68 (2017).
33. Li, J. *et al.* A high thermoelectric figure of merit ZT > 1 in Ba heavily doped BiCuSeO oxyselenides. *Energy Environ. Sci.* **5,** 8543 (2012).
34. Li, S. *et al.* Thermoelectric properties of CoSb3 with maize-like structure. *Phys. Status Solidi - Rapid Res. Lett.* **1,** 259–261 (2007).
35. Hsiao, C. L. & Qi, X. The oxidation states of elements in pure and Ca-doped BiCuSeO thermoelectric oxides. *Acta Mater.* **102,** 88–96 (2016).
36. Li, J. *et al.* $BaCu_2Se_2$ based compounds as promising thermoelectric materials. *Dalt. Trans.* **44,** 2285–2293 (2015).
37. Saini, S. *et al.* Terbium Ion Doping in Ca3Co4O9: A Step towards High-Performance Thermoelectric Materials. *Sci. Rep.* **7,** 44621 (2017).
38. Ren, G.-K. *et al.* Enhanced thermoelectric properties in Pb-doped BiCuSeO oxyselenides prepared by ultrafast synthesis. *RSC Adv.* **5,** 69878–69885 (2015).
39. Li, F., Wei, T.-R., Kang, F. & Li, J.-F. Enhanced thermoelectric performance of Ca-doped BiCuSeO in a wide temperature range. *J. Mater. Chem. A* **1,** 11942 (2013).
40. Li, F. *et al.* Polycrystalline BiCuSeO oxide as a potential thermoelectric material. *Energy Environ. Sci.* **5,** 7188 (2012).
41. Carvillo, P., Chen, Y., Boyle, C., Barnes, P. N. & Song, X. Thermoelectric Performance Enhancement of Calcium Cobaltite through Barium Grain Boundary Segregation. *Inorg. Chem.* **54,** 9027–9032 (2015).

42. Qi, X., Zeng, L., Wang, H., Liu, P. & Liu, Y. Thermoelectric properties of Ca3Co4O9 ceramics. *J. Wuhan Univ. Technol. Mater. Sci. Ed.* **25,** 287–290 (2010).
43. Schrade, M., Norby, T. & Finstad, T. G. Hall effect measurements on thermoelectric Ca3Co4O9: On how to determine the charge carrier concentration in strongly correlated misfit cobaltites. *J. Appl. Phys.* **117,** 205103 (2015).
44. Kenfaui, D. *et al.* Volume Texture and Anisotropic Thermoelectric Properties in Ca3Co4O9 Bulk Materials. *Mater. Today Proc.* **2,** 637–646 (2015).
45. Koumoto, K. *et al.* Thermoelectric ceramics for energy harvesting. *J. Am. Ceram. Soc.* **96,** 1–23 (2013).
46. Sootsman, J. R., Chung, D. Y. & Kanatzidis, M. G. New and old concepts in thermoelectric materials. *Angew. Chemie - Int. Ed.* **48,** 8616–8639 (2009).
47. Barreteau, C., Berardan, D. & Dragoe, N. Studies on the thermal stability of BiCuSeO. *J. Solid State Chem.* **222,** 53–59 (2015).
48. Vaqueiro, P., Guélou, G., Stec, M., Guilmeau, E. & Powell, A. V. A copper-containing oxytelluride as a promising thermoelectric material for waste heat recovery. *J. Mater. Chem. A* **1,** 520 (2013).
49. Butt, S. *et al.* Enhancement of thermoelectric performance in Cd-doped $Ca_3Co_4O_9$ via spin entropy, defect chemistry and phonon scattering. *J. Mater. Chem. A* **2,** 19479–19487 (2014).
50. Zhang, Y. F., Zhang, J. X., Lu, Q. M. & Zhang, Q. Y. Synthesis and characterization of Ca3Co4O9 nanoparticles by citrate sol-gel method. *Mater. Lett.* **60,** 2443–2446 (2006).
51. Koumoto, K., Terasaki, I. & Funahashi, R. Complex Oxide Materials for Potential Thermoelectric Applications. *MRS Bull.* **31,** 206–210 (2006).
52. Schulz, T. & Töpfer, J. Thermoelectric properties of Ca3Co4O9 ceramics prepared by an alternative pressure-less sintering/annealing method. *J. Alloys Compd.* **659,** 122–126 (2016).
53. Lin, Y. H. *et al.* High-temperature electrical transport behaviors in textured Ca 3Co4O9-based polycrystalline ceramics. *Appl. Phys. Lett.* **94,** 2–5 (2009).

54. Shikano, M. & Funahashi, R. Electrical and thermal properties of single-crystalline (Ca2CoO3)0.7CoO2 with a Ca3Co4O9 structure. *Appl. Phys. Lett.* **82,** 1851–1853 (2003).

55. Prasoetsopha, N., Pinitsoontorn, S. & Amornkitbamrung, V. Synthesis and thermoelectric properties of Ca 3Co 4O 9 prepared by a simple thermal hydro-decomposition method. *Electron. Mater. Lett.* **8,** 305–308 (2012).

56. Delorme, F., Ovono Ovono, D., Marudhachalam, P., Fernandez Martin, C. & Fraboulet, O. Effect of precursors size on the thermoelectric properties of Ca3Co4O9 ceramics. *Mater. Res. Bull.* **47,** 1169–1175 (2012).

57. Kenfaui, D. *et al.* Development of multilayer textured Ca 3Co 4O 9 materials for thermoelectric generators: Influence of the anisotropy on the transport properties. *J. Eur. Ceram. Soc.* **32,** 2405–2414 (2012).

58. Kang, M. G. *et al.* Post-calcination, a novel method to synthesize cobalt oxide-based thermoelectric materials. *Acta Mater.* **73,** 251–258 (2014).

59. Kenfaui, D., Chateigner, D., Gomina, M. & Noudem, J. G. Texture, mechanical and thermoelectric properties of Ca3Co4O9 ceramics. *J. Alloys Compd.* **490,** 472–479 (2010).

60. Brinks, P., Van Nong, N., Pryds, N., Rijnders, G. & Huijben, M. High-temperature stability of thermoelectric Ca<inf>3</inf>Co<inf>4</inf>O<inf>9</inf> thin films. *Appl. Phys. Lett.* **106,** 102–106 (2015).

61. Lin, Y. H. *et al.* High-temperature electrical transport and thermoelectric power of partially substituted Ca3Co4O9-based ceramics. *J. Am. Ceram. Soc.* **90,** 132–136 (2007).

62. Liu, Y., Lin, Y., Shi, Z., Nan, C. W. & Shen, Z. Preparation of Ca3Co4O9 and improvement of its thermoelectric properties by spark plasma sintering. *J. Am. Ceram. Soc.* **88,** 1337–1340 (2005).

63. Bhattacharya, S. *et al.* Low temperature thermopower and electrical transport in misfit Ca 3Co4O9 with elongated c-axis. *J. Phys. D. Appl. Phys.* **41,** (2008).

64. Madre, M. A. *et al.* Preparation of high-performance Ca3Co4O9 thermoelectric ceramics produced by a new two-step method. *J. Eur. Ceram. Soc.* **33,** 1747–1754 (2013).

65. Miyazaki, Y. *et al.* Low-Temperature Thermoelectric Properties of the Composite Crystal [Ca 2CoO 3.34] 0.614[CoO 2]. *Jpn. J. Appl. Phys.* **39,** L531–L533 (2000).
66. Van Nong, N., Pryds, N., Linderoth, S. & Ohtaki, M. Enhancement of the thermoelectric performance of p-type layered oxide Ca3Co4O9+δ through heavy doping and metallic nanoinclusions. *Adv. Mater.* **23,** 2484–2490 (2011).
67. Yudin, A. *et al.* Synthesis of hollow nanostructured nickel oxide microspheres by ultrasonic spray atomization. *J. Aerosol Sci.* **98,** 30–40 (2016).
68. Eslamian, M. & Ashgriz, N. Effect of Atomization Method on the Morphology of Spray-Generated Particles. *J. Eng. Mater. Technol.* **129,** 130 (2007).
69. Okuyama, K., Abdullah, M., Lenggoro, I. W. & Iskandar, F. Preparation of functional nanostructured particles by spray drying. *Adv. Powder Technol.* **17,** 587–611 (2006).
70. Nandiyanto, A. B. D. & Okuyama, K. Progress in developing spray-drying methods for the production of controlled morphology particles: From the nanometer to submicrometer size ranges. *Adv. Powder Technol.* **22,** 1–19 (2011).
71. Jayanthi, G. V., Zhang, S. C. & Messing, G. L. Modeling of solid particle formation during solution aerosol thermolysis: The evaporation stage. *Aerosol Sci. Technol.* **19,** 478–490 (1993).
72. Woermann, E. & Muan, A. Phase equilibria in the system CaO-cobalt oxide in air. *J. Inorg. Nucl. Chem.* **32,** 1455–1459 (1970).
73. Thanh, N. T. K., Maclean, N. & Mahiddine, S. Mechanisms of nucleation and growth of nanoparticles in solution. *Chem. Rev.* **114,** 7610–7630 (2014).
74. Carson, J. K., Lovatt, S. J., Tanner, D. J. & Cleland, A. C. Thermal conductivity bounds for isotropic, porous materials. *Int. J. Heat Mass Transf.* **48,** 2150–2158 (2005).
75. Lee, H. *et al.* Effects of nanoscale porosity on thermoelectric properties of SiGe. *J. Appl. Phys.* **107,** 1–7 (2010).
76. Mi, J. L., Zhu, T. J., Zhao, X. B. & Ma, J. Nanostructuring and thermoelectric properties of bulk skutterudite compound CoSb3. *J. Appl. Phys.* **101,** (2007).

77. Lemmon, E. W. & Jacobsen, R. T. Viscosity and Thermal Conductivity Equations for Nitrogen, Oxygen, Argon, and Air.PDF. **25,** (2004).
78. Raghavan, S., Wang, H., Dinwiddie, R. B., Porter, W. D. & Mayo, M. J. The effect of grain size, porosity and yttria content on the thermal conductivity of nanocrystalline zirconia. *Scr. Mater.* **39,** 1119–1125 (1998).
79. Medlin, D. L. & Snyder, G. J. Interfaces in bulk thermoelectric materials. A review for Current Opinion in Colloid and Interface Science. *Curr. Opin. Colloid Interface Sci.* **14,** 226–235 (2009).
80. Zhang, R. Z., Wang, C. L., Li, J. C. & Koumoto, K. Simulation of thermoelectric performance of bulk SrTiO3 with two-dimensional electron gas grain boundaries. *J. Am. Ceram. Soc.* **93,** 1677–1681 (2010).
81. Dresselhaus, M. S. *et al.* New directions for low-dimensional thermoelectric materials. *Adv. Mater.* **19,** 1043–1053 (2007).
82. Lee, M.-J. *et al.* Thermoelectric materials by using two-dimensional materials with negative correlation between electrical and thermal conductivity. *Nat. Commun.* **7,** 12011 (2016).
83. Mao, J., Liu, Z. & Ren, Z. Size effect in thermoelectric materials. *npj Quantum Mater.* **1,** 16028 (2016).
84. Balandin, A. & Wang, K. L. Significant decrease of the lattice thermal conductivity due to phonon confinement in a free-standing semiconductor quantum well. *Phys. Rev. B - Condens. Matter Mater. Phys.* **58,** 1544–1549 (1998).
85. Ning, H. *et al.* Enhanced thermoelectric performance of porous magnesium tin silicide prepared using pressure-less spark plasma sintering. *J. Mater. Chem. A* **3,** 17426–17432 (2015).